Marie-Theres Zechner, BSc

The Parkinson's Disease-Associated Protein LRRK2 Inhibits Autophagy

MASTER'S THESIS

to achieve the university degree of

Master of Science

Master's degree programme: Biochemistry and Molecular Biomedical Sciences

submitted to

Graz University of Technology

Supervisor

Assistant Prof. Dr. Sabrina Büttner

Institute of Molecular Biosciences
(University of Graz)

Graz, November 2017

AFFIDAVIT

I declare that I have authored this thesis independently, that I have not used other than the declared sources/resources, and that I have explicitly indicated all material which has been quoted either literally or by content from the sources used. The text document uploaded to TUGRAZonline is identical to the present master's thesis.

30.11.2017
Date


Signature

Acknowledgements

Thank you to Sabrina for letting me work in her lab group and providing knowledge and support.

Thank you to Andreas for teaching me the techniques and providing advice and information.

Thank you to Lisi, the best partner one could ask for, a people I'd take a bullet for A-lister, I know you always have my back.

Thank you to Lukas for being a delightful human being made of sunshine and all things good.

Thank you to everyone who works on the ground floor of the Institute of Molecular Biosciences for a supportive and cool work environment (and cake). Thank you to Michelle for classing up L6, to Sarah for letting me stalk and talk, to Ronny for being hilarious, to Nadine for being amazing and to Anna for making my day.

Thank you to Thomas Schnedlitz. You know why.

Thank you to the nerds who lurk around Körblergasse 30, for reminding me that life outside the lab exists and is pretty good actually.

Thank you to Nina and Kristin of the online emotional support crew.

Shout out to the great people at Offenes Labor Graz for making me laugh and reminding me why science is important to humanity as a whole and so, so worthwhile.

Last but not least und im Herzen vor allem: Danke an meine Familie, die mir alles ermöglicht und mich immer unterstützt hat.

Abstract

Mutations in the leucine-rich repeat kinase 2 (LRRK2) have been linked to late-onset, autosomal dominant, familial Parkinson's disease (PD). LRRK2 toxicity has been shown to cause defects in the autophagic pathway in both yeast and neuronal models. Autophagy is a main intracellular degradation system and an essential pathway for reducing pathogenic effects seen in proteinopathies like PD. Furthermore, LRRK2 has been proposed to interact with the PD-related protein α-synuclein, the main component of the protein aggregates found in PD patients. This study further analyses the mechanism by which mutations in LRRK2 affect autophagy in yeast and investigate a possible interaction between LRRK2 and α-synuclein. The impairment of autophagy by LRRK2 shown in other model systems was confirmed in our ageing yeast model and pharmacological induction of autophagy was shown to reduce LRRK2 toxicity. The autophagy block was not caused by changes in vacuolar acidification. Overexpression of the vacuolar protease Pep4 proved to be protective against LRRK2-induced cell death, while cellular protein levels of Pep4 were shown to be unaffected by LRRK2. α-Synuclein was successfully co-expressed but showed no co-toxicity with LRRK2 in this model.

Kurzzusammenfassung

Mutationen in der leucine-rich repeat kinase 2 (LRRK2) sind mit familiärem Morbus Parkinson in Verbindung gebracht worden. Es wurde gezeigt, dass LRRK2 Toxizität sowohl in Hefe als auch in Neuronen zu Defekten in Autophagie Stoffwechselwegen führt. Autophagie ist ein wichtiger Bestandteil des intrazellulären Abbaus von Proteinen und essentiell um pathogene Effekte zu verhindern, die in Proteinopathien wie Parkinson auftreten. Des Weiteren wurde spekuliert, dass LRRK2 möglicherweise mit α-Synuclein interagiert, welches der Hauptbestandteil der mit Morbus Parkinson assoziierten Proteinaggregate ist. Diese Studie versucht neue Erkenntnisse über die Effekte von LRRK2 und Mutationen in *LRRK2* auf Autophagie zu gewinnen und untersucht die potentielle Interaktion von LRRK2 und α-Synuclein. Eine Inhibierung der Autophagie durch LRRK2, wie bereits in anderen Modelsystem gezeigt, konnte in unserem alternden Hefemodel bestätigt werden und eine pharmakologische Induktion von Autophagie reduzierte LRRK2 Toxizität. Der Grund für die Blockade lag nicht in Veränderungen des pH-Wertes der Vakuole. Überexprimieren der vakulären Protease Pep4 führte zu reduzierter LRRK2 Toxizität, wobei LRRK2 keinen Effekt auf die basale zelluläre Proteinmenge von Pep4 hatte. Die Koexpression von α-Synuclein und LRRK2 war erfolgreich, jedoch wurde keine synergistische Toxiziät festgestellt.

TABLE OF CONTENTS

1 INTRODUCTION

1.1 Parkinson's Disease

Parkinson's disease (PD) is a complex neurological disorder. It is one of the most common neurodegenerative diseases worldwide, second only to Alzheimer's disease[1,2,3]. Its prevalence rises with age. Studies have found that while 41 per 100,000 in individuals aged 40 to 49 years develop the disease, this number rises to 1,903 per 100,000 for individuals that are 80 years and older[2]. Its costs are high regarding both human quality of life and economics[4,5].

The hallmark of PD are its motor symptoms. Patients suffer from a slowness of movement, muscular rigidity, resting tremor and an instability of gait and posture[6]. Non-motor symptoms add to the deterioration of health. These include cognitive impairment, depression, anxiety, sleep disorders, olfactory and autonomic dysfunction[6,7] and commonly start to occur in the early stages of PD[7].

There is as of yet no treatment that can stop the progression of PD. Available drugs primarily help to alleviate the severity of the condition[8]. In order to improve medical therapy, it is vital that we gain a better understanding of the pathogenesis and pathology of the disease.

The main pathological feature of PD is the loss of dopaminergic neurons in the substantia nigra pars compacta (SNc). The SNc is a component of the basal ganglia, which is located in the midbrain. As part of the basal ganglia-thalamocortical circuitry, basal ganglia involvement has been implicated in multiple motor behaviours, including action selection, preparation, execution and sequencing of movement and control of movement parameters[9]. The signalling of the dopaminergic neurons of the SNc to the striatum constitutes a regulatory part of this pathway. In accordance, studies have shown that the loss of these neurons in PD is likely what leads to its motor symptoms[10]. However, it is estimated that approximately 60% of SNc dopaminergic neurons are lost before motor symptoms occur[11]. Additionally, neurodegeneration is not confined to the SNc. Other brain areas strongly affected include the amygdala, locus ceruleus, basal nucleus of Meynert, hypothalamus and medullary tegmentum[12], all of which are anatomically interconnected[13].

At least partially responsible for the loss of neurons is a factor PD shares with other neurodegenerative diseases: Aggregation of abnormally folded proteins. In PD these inclusions are referred to as Lewy bodies or Lewy neurites[14], depending on whether they are located in the neuronal soma or processes. They are found in patients' brains and spinal cords, but also more widespread in the peripheral and enteric nervous system[15]. Lewy pathology is not restricted to PD; it is also present in other diseases such as dementia with Lewy bodies[16] and

multiple system atrophy[17]. These disorders are classified as "synucleinopathies", a term referring to the main component present in Lewy bodies – alpha-synuclein (αSyn)[18].

The protein αSyn is composed of 140 amino acids, structured in a basic N-terminus, a central hydrophobic core and an acidic C-terminus[19]. Physiologically, it is located at presynaptic terminals[20]. Its function is thus far uncertain[21]; however, it has been proposed to be involved in mediating the formation of the SNARE-complex[22], which is necessary for vesicle docking and membrane fusion – and therefore the release of neurotransmitters into the synaptic cleft. Pathologically, αSyn becomes insoluble and forms unbranched filaments[16]. What exactly prompts this aggregation and what stops cellular clearance mechanisms from effectively removing it remains unclear[23]. Although αSyn aggregation is a defining feature of PD, there have been cases of monogenic PD where no Lewy bodies were present[24,25]. A definitive causal relation has yet to be established[26].

Most cases of PD are idiopathic – they occur without identifiable cause. Meta-analysis has suggested several environmental risk factors, including exposure to pesticides, prior head injury, usage of β-blockers, rural living and work in agriculture[27,28]. However, these factors appear to only slightly heighten the probability of developing the disease.

Mutations have been identified as a risk factor for idiopathic PD, as well as the cause of hereditary monogenetic forms of the disease. Only approximately 3-5% of idiopathic cases and 30% of familial cases are attributed to monogenetic mutations[29]. Nonetheless, the discovery of these mutations has made it possible to determine molecular pathways that are likely to be involved in PD, including impairment of synaptic exocytosis and endocytosis, endosomal trafficking, mitochondrial maintenance and protein degradation via autophagy or the ubiquitin-proteasome pathway[30].

The first PD-related mutation to be discovered was located in *SNCA*, the gene encoding for αSyn[31]. Since then, several additional mutations in *SNCA* associated with idiophathic or autosomal-dominant PD have been identified, including missense mutations as well as multiplications of the gene locus[21]. The most frequent cause of dominantly inherited PD are mutations in *LRRK2*[32], which encodes for the Leucine-rich-repeat kinase 2 (see below). Further autosomal dominant mutations occur in *VPS35*[33], *EIF4G1*[34], *DNAJC13*[35] and *CHCHD2*[36]. VPS35 and DNAJC13 are involved in endosomal protein trafficking; EIF4G1 is a translation initiation factor and CHCHD2 a regulator of mitochondrial metabolism[37]. Mutations in *parkin* are the most common cause of early onset recessive familial PD[32,38]. Other recessive mutations are located in *PINK1*[39] and *DJ-1*[40]. Both parkin and PINK1 are important for mitophagy, while DJ-

1 is a sensor of oxidative stress. However, this list of genetic loci is not exhaustive. Genome wide association studies have identified multiple additional potential candidate genes[32] that may offer yet further insights into PD pathology.

1.2 Leucine-Rich Repeat Kinase 2

Mutations in *LRRK2* are the most frequent cause of autosomal dominant PD[32]. This gene encodes for the Leucine-rich repeat kinase 2 (LRRK2), a large multi-domain protein composed of 2527 amino acids. LRRK2 exhibits dual enzymatic functions, conferred by a Ras of complex (Roc) GTPase domain and a serine/threonine protein kinase domain. The two catalytic sites are linked by a C-terminal of Roc (COR) domain and flanked by several protein interaction domains including armadillo repeats, ankyrin repeats and leucine-rich repeats at the N-terminus and a WD40 domain at the C-terminus[41] (Figure 1). It has been shown that LRRK2 forms dimers under native conditions[42].

Figure 1: The domain structure of LRRK2. ARM = armadillo repeats, ANK = ankyrin repeats, LRR = leucine-rich repeats, COR = C-terminal of Roc.

LRRK2 is expressed in several brain regions, including the striatum, cortex, hippocampus, cerebellum and the dopaminergic neurons of the SNc[43,44], as well as in the lungs[44], kidneys[44] and cells of the immune system[45]. Within cells, LRRK2 has been shown to localise at intracellular membranes such as the outer mitochondrial membrane, or at the membranes of the lysosome, endoplasmic reticulum and Golgi apparatus, as well as at vesicular structures like endosomes, autophagosomes, multivesicular bodies and transport vesicles[46,47]. LRRK2 is typically also present in Lewy bodies[48] – however, not all cases of LRRK2-associated PD feature Lewy body pathology[25].

Systematic mutation screens have shown that *LRRK2* mutations are found in approximately 5-10% of patients with autosomal dominant PD[49,50,51,52], 3.6% of patients with idiopathic PD and 1.8% of healthy controls[53]. 80 putatively PD-related mutations within *LRRK2*[54] have been identified. Most of these are missense mutations, where a single nucleotide change leads to the substitution of one amino acid in the protein. However, at this time only few of the mutations have been shown to lead to pathogenic consequences[55]. The most frequent of these is G2019S[32],

which is situated in the kinase domain and increases kinase activtiy[56,57]. G2019S-related PD cases are usually clinically indistinguishable from idiopathic PD, including late onset and the presence of Lewy bodies[58,59]. Another mutation, I2020T occurs at the adjacent residue. Its effects on kinase activity are still ambiguous[60,61]. The second most commonly mutated residue is Arg-1441, situated in the Roc GTPase domain. Three different substitutions have been observed: R1441G, R1441C and R1441H. R1441H has been shown to increase GTP-binding affinity[62], while R1441C decreases GTPase activity[63]. The pathogenic Y1699C polymorphism in the COR region between the kinase and GTPase domains has been reported to decrease GTPase activity as well[64]. Further pathogenic mutations are more rare; G2385R in the WD40 domain and R1628P in the COR domain increase PD risk in Asian populations[65,66,67], while the N1437H substitution in the GTPase domain does so in Scandinavian families[68]. Studies show that G2385R leads to decreased kinase activity[69], while R1628P increases it[70]. N1437H appears to increase both GTP-binding and kinase activity[68].

In addition to offering a better understanding of PD pathology, discovery of these mutations has also revealed potential pharmacological targets. The fact that the G2019S mutation causes increased kinase activity has led to a search for kinase inhibitors as an avenue of treatment[71]. However, R1441C, R1441G and Y1699C have been linked to cytotoxicity as well[56,72], suggesting that kinase activity is not the only important factor in LRRK2 toxicity.

Models to study LRRK2 have been established in several organisms, including yeast, *Drosophila melanogaster*, *Caenorhabditis elegans*, zebrafish, rodents and patient-derived induced pluripotent stem cells (iPSC). While none of these models has managed to fully replicate PD phenotypes, each offers different advantages[73]. Yeast provides a fast and cost effective way to screen for modifiers of LRRK2 toxicity or observe the impact of LRRK2 pathobiology on conserved pathways (see below). *Drosophila* and *C. elegans* are similarly convenient and have the advantage of an existing nervous system, but lack complexity in their neural circuitry and have no true LRRK2 homolog. This among other reasons makes it necessary to confirm findings made in lower organisms in mammalian models. In addition, models using iPSC make it possible to directly study the consequences of *LRRK2* mutations in human physiology.

The exact function of LRRK2 is yet unknown, although its kinase activity suggests a role in cellular signalling pathways. The kinase activity has been found to be required for LRRK2 mutant neurotoxicity in cell culture[74,75] and is dependent on dimerisation[76] and membrane localisation[77]. Several potential substrates have been suggested, but have yet to be validated in a physiological context[73,78]. The only currently recognised substrate for LRRK2 is itself[42]. LRRK2 has been shown to autophosphorylate more than 20 serine and threonine residues in

vitro[42,79,80,81], although not all of these have been replicated in vivo. Most of the autophosphorylation sites are situated in the GTPase domain, with a few residing in the COR or kinase domain instead. Notably, there are further phosphorylation sites prior to the GTPase domain that are not sites for autophosphorylation and are used as a measure of kinase activity[78]. Changes in its phosphorylation status have also been connected to LRRK2's membrane localisation[77].

Another open question is the interplay between the kinase and LRRK2's other enzymatic function – do they oppose each other, or facilitate the same outcome? The Ras GTPase family undergo guanine-nucleotide-dependent conformational changes, enabling them to play the function of a molecular switch in signalling pathways. It has been proposed that LRRK2's GTPase acts in a similar fashion[82,83]. It is likely that the kinase domain has a regulatory function on the GTPase, as autophosphorylation in the GTPase domain regulates GTP binding[84]. Likewise, kinase activity requires an intact GTPase domain[85] and may be regulated by GTP binding[86] – although it has also been observed that the kinase activity is not inhibited if GDP is present and not enhanced in the presence of GTP or non-hydrolysable GTP[85,87], making this connection uncertain.

In addition to the many putative substrates, LRRK2 has been implicated in a wide variety of cellular pathways[78,88]. These include mitogen-activated protein kinase pathways, immune-cell-specific pathways, cytoskeleton dynamics, mitochondrial dynamics, vesicular trafficking and autophagy.

LRRK2 has been linked to autophagy in multiple model systems, but the details of this connection remain elusive. Studies in mice have shown an increase of autophagosomes in the cortex of mice with the R1441C mutation and in the cortex and striatum of mice carrying the G2019S mutation[89]. In *C. elegans*, autophagy genes were found to be regulated in coordination with LRRK2[90]. The connection has been studied in several cell lines as well: Blocking autophagy in SHSY5Y neuroblastoma cells overexpressing the G2019S mutant protein alleviated its toxicity[91]. LRRK2 wild type or G2019S overexpression led to an accumulation of autophagosomes in several cell lines[92]. Contrarily, studies of LRRK2 mutations in human fibroblasts showed the G2019S mutation increased autophagy[93], while LRRK2 with G2019S, Y1699C or R1441G mutations impaired the autophagy response to starvation[94]. LRRK2 inhibition stimulated autophagy in human neuroglioma cells[95] and SH-SY5Y cells[96]. A knockdown of LRRK2 induced autophagy in HEK293 cells[47] and the inhibition of LRRK2 increased autophagy in astrocytic cell models in a non-canonical, mammalian target of

rapamycin independent manner[97]. Finally, expression of the G2019S mutant decreased autophagy in iPSC-derived human dopaminergic neurons[98].

Further research is needed to clarify the link between LRRK2 and autophagy. One problem is that it is not known whether LRRK2 has a different role in different model systems and/or cell lines. Another unresolved issue is if LRRK2 interacts with autophagy pathways directly or triggers downstream effects that influence autophagy. Furthermore, it is unclear whether LRRK2 is involved in autophagy regulation under healthy conditions or the connection is only established during disease[99].

1.3 Yeast as a Model for Neurotoxic Cell Death

The budding yeast *Saccharomyces cerevisiae* is a model organism commonly used in research targeted at understanding protein function and cellular pathways. This is possible due to a high degree of conservation of basic molecular function and fundamental pathways with the mammalian system. Although yeast lacks the complexity of mammalian cells and findings have to be validated in higher organisms, it offers significant advantages as well: Yeast is easy to cultivate and allows for comparatively simple genetic manipulation and genome-wide screening.

The hallmark of most neurodegenerative diseases are protein aggregations, which are thought to cause cell death[100]. The implicated cell death pathways – necrosis, apoptosis[101], oxidative stress and mitochondrial dysfunction[102], ER-stress mediated cell death[103] – are largely conserved in yeast. Although autophagic pathways are conserved in yeast (see below), it has yet to be explored whether autophagic cell death occurs in yeast as well[101].

Yeast models have already been successfully established for several neurodegenerative diseases, including α-synucleinopathies, polyglutamine disorders, β-amyloid disorders and tautophaties[104]. Although PD-related models in yeast have thus far largely focused on αSyn[105], a few attempts have been made to study LRRK2 as well. These have been mainly focused on elucidating the GTPase function. One study was able to show that the GTPase domain has a key role in mediating LRRK2 toxicity[106]. Notably, endocytic vesicular trafficking to the vacuole and autophagy were impaired in this yeast model. Further studies were able to demonstrate that GCS1 functions as a GTPase activating protein for LRRK2[107], which has been confirmed in the mammalian system for its ortholog ArfGAP1[108]. In addition, a study investigating LRRK2 mutants in the context of oxidative stress observed that only the LRRK2 wild type, but not pathogenic mutants, protect against reactive oxidant species in yeast[109].

1.4 Autophagy

Autophagy is one of the molecular pathways that have been reported to be dysfunctional in PD[30]. Evidence from several studies suggests that LRRK2 interferes with autophagic processes[99,110], but it is as of yet unknown how this interference occurs.

The term autophagy refers to a group of degradation processes that can be separated into the classifications of macroautophagy, microautophagy and chaperone-mediated autophagy[111,112]. In macroautophagy double-membrane vesicles called autophagosomes engulf cellular components and transport them to the vacuole, where the cargo is degraded after fusion of the autophagosomal outer membrane with the vacuole (Figure 2). This can happen selectively or non-selectively. By contrast, in microautophagy the cargo is engulfed directly at the vacuole via invagination, protrusion, and septation of the vacuolar membrane. Microautophagy can occur selectively or non-selectively as well, with selective microautophagy playing an important role in the turnover of mitochondria, peroxisomes and parts of the nucleus. Chaperone-mediated autophagy differs in that no new vesicular structure is formed. Instead, proteins are delivered directly into the lysosome through a protein-translocation complex. It is uncertain whether chaperone-mediated autophagy is present in lower organisms[113].

As macroautophagy is the relevant pathway to this thesis, it will be the focus of this chapter and hereafter be referred to as autophagy. While the pathways are largely conserved from yeast to the mammalian system[111], there are differences at certain stages of the process as well as in nomenclature. By reason of *S. cerevisiae* being the model organism of choice for this thesis, this chapter will describe yeast autophagy.

While the cell's other main degradation mechanism, the ubiquitin-proteasome system, is required to remove most short-lived, misfolded or damaged proteins, autophagy is responsible for the degradation of long-lived proteins, large protein complexes and damaged organelles[114].

Autophagy induction is regulated by the Atg1 complex and occurs at what is referred to as the phagophore assembly site (PAS)[115]. In the following nucleation stage, the Atg14-containing class III phosphatidylinositol 3-kinase complex I is recruited to the PAS[116]. In a process that has yet to be fully elucidated, a double-membrane precursor structure called the phagophore is created at the PAS[117]. Next, the phagophore is expanded. This requires two ubiquitin-like protein conjugation complexes involving the proteins Atg12 and Atg8[118]. Atg12 is activated by Atg7 and conjugated to Atg5 by Atg10[119]. The function of the Atg12 complex is unclear; however, it is involved in recruiting the Atg8 conjugation system[120]. The Atg4 cysteine protease cleaves the C-terminal arginine off Atg8, whereupon it is activated by Atg7 and transferred to

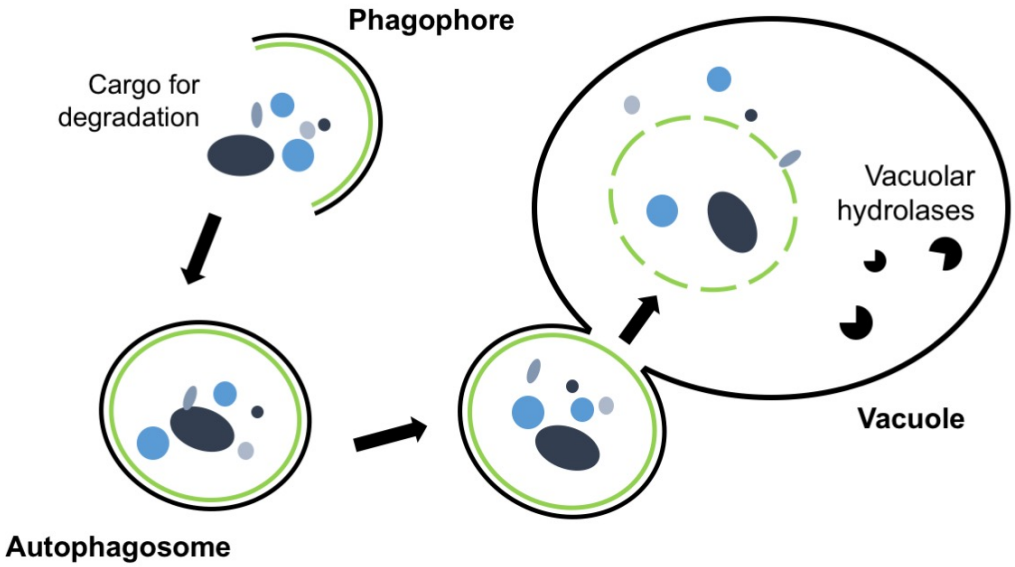

Figure 2: Macroautophagy in yeast. A phagophore forms and engulfs the cargo. The fully formed double-membrane vesicle called the autophagosome transports the cargo to the vacuole where the outer membrane of the autophagsome fuses with the vacuolar membrane. The inner membrane and the cargo are degraded by vacuolar hydrolases.

Atg3. Atg3 then forms a covalent bond between the C-terminus of Atg8 and phosphatidylethanolamine (PE) on the phagophore membrane[121]. Atg8-PE is involved in cargo recognition and may contribute to membrane curvature[122]. Atg9 is thought to play a key role in phagophore expansion as well[123], although it is yet uncertain exactly how.

Once the phagophore has completely engulfed the cargo and its membrane is closed around it, it is considered a fully formed autophagosome. The size of the autophagosome varies depending on its cargo but is typically between 0.3 and 0.9 µm[124]. Tethering and fusion of the outer autophagosomal membrane with the vacuole requires a variety of factors including the Rab GTPase Ypt7[125] and several SNARE proteins such as Vam3[126], Vam7, Vti1 and Ykt6[112]. In addition, vacuolar protease activity and acidification are necessary[127]. Finally, after the fusion the lipase Atg15 dismantles the inner autophagosomal membrane[128] and the cargo is degraded by vacuolar hydrolases.

As an important cellular process, autophagy is tightly regulated by epigenetic, transcriptional and post-transcriptional mechanisms[117]. While autophagy is active constitutively at a basal level, it can be massively induced under nutrient starvation. The cell's main integrator of

nutrient-derived signals and a negative regulator of autophagy is the serine/threonine protein kinase target of rapamycin (TOR)[129,130].

Two TOR complexes have been identified in yeast: The TOR complex 1 (TORC1) and TOR complex 2 (TORC2). Both TORC1 and TORC2 redundantly control autophagy, progression of the cell cycle, ribosome biogenesis, transcription regulation and amino acid uptake by permeases[129,131]. TORC2 additionally regulates the polarization of the actin cytoskeleton and sphingolipid biosynthesis[132]. Rapamycin – one of the most common ways to induce autophagy in laboratory settings next to nitrogen starvation – only inhibits the signalling branch shared by TORC1 and TORC2[129].

Under nutrient rich conditions, TOR is active and upregulates anabolic pathways while also repressing processes necessary for the response to nutrient deprivation. Under starvation conditions, TOR is inactivated. It no longer stimulates pathways for cell growth and stops repressing pathways like autophagy, leading to their initiation[131].

TOR inhibits autophagy via Atg13, which is part of the Atg1 complex (see above). When TOR is active, it phosphorylates Atg13 at several Ser residues[133], preventing its interaction with the Atg1 complex. When TOR is inhibited, Atg13 is dephosphorylated and becomes active, leading to the assembly of the Atg1 complex and initiation of autophagy[134]. In addition, TOR further controls autophagy by regulating transcription factors for autophagy related genes[117].

1.5 The Yeast Vacuole and Vacuolar Proteases

The yeast vacuole is an acidic organelle that shares many functions with the mammalian lysosome[135]. Both compartments are involved in the degradation of cargo delivered via endocytosis or autophagy. Both then supply the degradation products for the synthesis of new macromolecules. Unlike the lysosome, the vacuole also carries out a variety of additional functions. It stores amino acids, ions and metals and recycles them to the cytosol when it becomes necessary. Furthermore, it is used to sequester toxic molecules.

This myriad of functions demands a highly flexible organelle that can adapt to the cellular environment as needed[135,136]. Thus, its morphology is dynamic, allowing for fission and fusion of vacuolar compartments amongst each other as well as fusion with cargo-carrying vesicles. Yeast cells typically contain multiple intermediately sized vacuolar lobes during exponential growth. Upon entering the stationary phase, or under nutrient deprivation, these lobes combine to form one larger vacuole. By contrast, under osmotic stress conditions the vacuole undergoes fission into numerous smaller vesicles. A low vacuolar pH is maintained by the V-

ATPase protein complex actively pumping protons into the organelle[137]. This is vital for the proper function and localisation of vacuolar proteins[138].

The proteins of the vacuole can be grouped into hydrolases and transporter proteins. Proteases are part of the former; they perform protein breakdown and can be either membrane-bound or solulable[136]. They are trafficked to the vacuole in a zymogen precursor form that has to be activated by a complex cascade resulting in proteolytic cleavage to remove a propeptide[139]. A key enzyme in this cascade is the protease Pep4[139,140]. While Pep4 itself autoactivates itself at low pH[139,141], other proteases such as proteinase B, carboxypeptidase Y and aminopeptidase I are dependent on it for activation. The proteases typically function with broad substrate specificity[136]. Both extracellular and intracellular proteins are trafficked to and degraded in the vacuole, with protein degradation occurring both constitutively and as a stress response[135].

1.5 A New Yeast Model for LRRK2

For my work on this thesis, I used a *S. cerevisiae* model previously established in our group to explore the mechanisms of LRRK2 toxicity.

This model analyses the impact of LRRK2 on yeast cells in the context of a chronological ageing. Chronological ageing examines the survival of yeast cells in the postdiauxic and stationary phase and is used as a model for post-mitotic, non-dividing cells in tissues of higher eukaryotes[142]. As the expression of full length human LRRK2 in yeast reportedly led to the formation of insoluble LRRK2 aggregates that failed to affect yeast viability[106], we examined a fragment consisting of the GTPase, COR and kinase (GCK) domains. The pYES2/CT plasmid was used for heterologous overexpression. In addition to the wild type form, we also looked at four mutated GCK domains, generously provided by Darren Moore[106]: R1398L, K1347A, G2019S and TripKN (Table 1, Figure 3). The G2019S mutation occurs in the kinase domain of LRRK2 in patients suffering from PD (see above). The other mutations have not been found in PD patients, but provide an opportunity to study the effects that changes in the enzymatic domains may exert upon LRRK2 function and toxicity. TripKN is another mutation affecting the kinase domain; the other two mutations affect the GTPase domain instead. The empty vector as well as pYES2/CT expressing β-galactosidase (LacZ) functioned as controls. LacZ is approximately of the same size as the GCK fragment while likely having no active function in yeast itself and is used to account for ER stress that might be caused by the overexpression of any protein.

Table 1: Analysed GCK domain mutations and their effect on the enzymatic functions.

Mutation	Effect
R1398L	enhanced GTPase
K1347A	impaired GTPase
G2019S	enhanced kinase
TripKN	impaired kinase

Figure 3: The LRRK2 GCK fragment and the mutations analysed in this study.

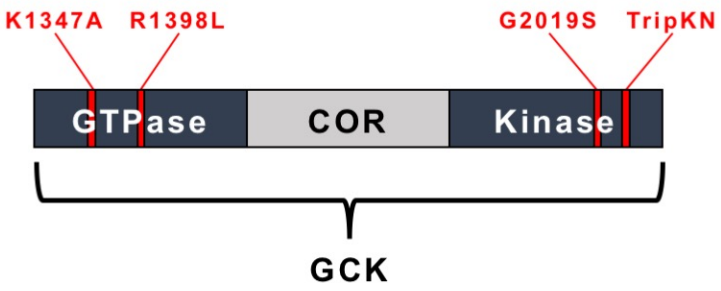

The expression of the GCK fragments as well as the LacZ control was confirmed via immunoblotting and consecutive detection of their V5-tag (Figure 4B).

Throughout the chronological ageing, cell death was monitored by testing for membrane integrity using flow cytometry to quantify propidium iodide (PI) stained cells (Figure 4A). The effects of LRRK2 toxicity were observable at approximately 40 hours after induction of LRRK2 expression. After 72 hours, the effect of LRRK2 on cell viability became apparent; cells expressing LRRK2 exhibited increased loss of membrane integrity and thus cell death compared to cells expressing LacZ. While there was no significant difference in cell death between the wild type form and the mutations affecting the kinase domain (G2019S, TripKN), or the mutation that impairs the GTPase function (K1347A), the mutation that enhances GTPase function (R1398L) was less toxic in this model.

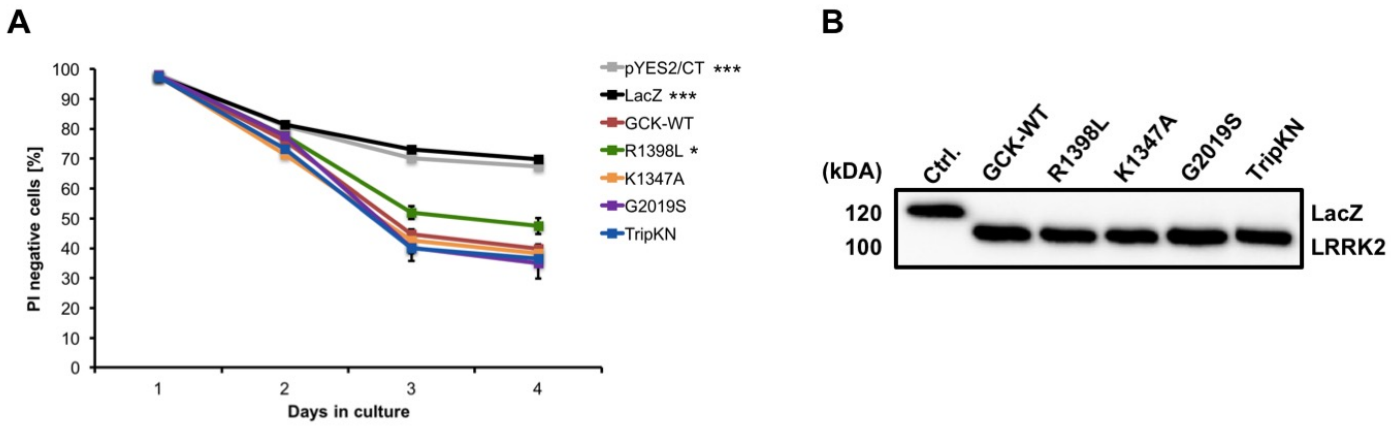

Figure 4 A model for LRRK2 toxicity in yeast cells heterologously expressing human LRRK2-GCK in its wild type form (GCK-WT) and several mutant alleles (R1398L, K1347A, G2019S, TripKN) compared to cells expressing LacZ and the empty vector (pYES2/CT). (**A**) Flow cytometric quantification of PI stained cells measuring cell death over a period of 4 days after induction of LRRK2-GCK expression. Mean ± S.E.M., $n = 4$, *** = $P < 0.001$, * = $P < 0.05$. (**B**) Immunoblot analysis expression control of LacZ and LRRK2-GCK.

1.6 Aim of This Study

The aim of this study was to further analyse the mechanism by which LRRK2 and its mutations affect autophagy in yeast and investigate a possible interaction between LRRK2 and αSyn.

2. Materials

2.1 Laboratory Equipment

The laboratory equipment used during research for this thesis is listed in Table 2.

Table 2: Equipment used during laboratory work.

Equipment	Specification
96 deep well plates	VWR
Analytical balance	Kern & Sohn GmbH, Germany
Autoclaves	Systec GmbH, Germany
Cell counter	CASY™, Schärfe Systems
Centrifuge (for FACS plates, 15 mL / 50 mL flasks)	Sigma 3-18K
Centrifuge (for reaction tubes)	5415 R, Eppendorf AG, Germany
ChemiDoc™ Touch	Bio-Rad Laboratories GesmbH
Colony counter	Olli MBS counter 3.0, LemnaTec Microbio GmbH
Current source	Bio-Rad Laboratories GesmbH
Electroporator	Eppendorf AG, Germany
FACS plates	Greiner
Flasks (15 mL / 50 mL)	Sarstedt AG & Co, Germany
Flow Cytometer	FACSAria™, BD Biosciences, Austria
Fluorescence microscope	Axioskop microscope, Zeiss, Austria
Freezer (-20°C)	Liebherr
Freezer (-80°C)	Forma Scientific and Sanyo
Gel camber	Bio-Rad Laboratories GesmbH
Magnetic stirrer	IKAMAG RCT (IKA)
Multi-pipettes	Eppendorf, Gilson and Matrix (Thermo Scientific)
NanoDrop	ND-1000, PeqLab
pH meter	Methrom
Photometer	DU 730 UV/Vis Spectrophotometer, Beckman Coulter
Pipette tips	Eppendorf AG, Germany
Pipettes	Gilson, Inc., USA
Platform shaker	Promax 2020, Heidolph
Reaction tubes	Eppendorf AG, Germany
Shaker for flasks	Multitron II, Infors H'T
Syringe	Hamilton
Thermomixer	Eppendorf AG, Germany
Vortex Genie 2	Scientific Industries, Inc., USA
Western Blotting system	Amershan Biosciences

2.2 Strains and Plasmids

Experiments were carried out in the *S. cerevisiae* strain BY4741 (MATa *his3*Δ1 *leu2*Δ0 *met15*Δ0 *ura3*Δ0) obtained from Euroscarf. In addition to the wild type, BY4741 harbouring endogenously GFP-tagged Atg8 (provided by Andreas Aufschnaiter), endogenously HA-tagged Pep4[143] or the vectors pESC-His empty, pESC-His expressing FLAG-tagged Pep4[144], pUG23-His empty (expressing free GFP) or pUG23-His expressing EGFP-tagged α-Synuclein[145] were used.

In each case, clones containing pYES2/CT expressing V5-tagged LacZ or V5-tagged LRRK2-GCK in the wild type variant (GCK-WT) or several mutant alleles (R1398L, K1347A, G2019S, TripKN) through a GAL 1 promotor (plasmids provided by Darren Moore[106]) were analysed. A summary can be found in Table 3.

Plasmids were amplified in *Escherichia coli* strain XL-1.

Table 3: Genotype modifications and plasmids used for *S. cerevisiae* BY4741. For each strain, clones containing pYES2/CT expressing $LacZ^{V5}$ or $LRRK2\text{-}GCK^{V5}$ in the wild type variant (GCK-WT) or several mutant alleles (R1398L, K1347A, G2019S, TripKN) were analysed (1st plasmid).

Strain	Genotype	2nd Plasmid	Plasmid Description
BY4741	MATa *his3*Δ1 *leu2*Δ0 *met15*Δ0 *ura3*Δ0 (WT)	-	-
BY4741	as above	pESC-His	HIS-marker, no insert
BY4741	as above	pESC-His	HIS-marker, Pep4 insert, galactose-induced glucose-repressible GAL10 promotor, C-terminal FLAG-tag
BY4741	as above	pUG23	HIS-marker, no insert (expressing C-terminal EGFP-tag), methionine-repressible MET25 promoter
BY4741	as above	pUG23	HIS-marker, α-Synuclein insert, C-terminal EGFP-tag, methionine-repressible MET25 promoter
BY4741	as WT, *GFP:ATG8*	-	-
BY4741	as WT, *PEP4:HA*	-	-

2.3 Growth Media

Growth media were prepared using double distilled water. Sterilisation was performed using a CertoClav or autoclave steriliser for 25 minutes at 121°C. *S. cerevisiae* cells were primarily grown on synthetic minimal medium (SMD/SMG), with the media lacking the amino acid(s) used as plasmid selection marker(s). Amino acid mixes were produced as 10x stock and autoclaved separately. Yeast peptone dextrose medium (YPD) was used to grow *S. cerevisiae* cells without selection marker carrying plasmids for transformations. *E.coli* cells were grown on lysogeny broth medium (LB). The composition of the media used is listed in Table 4.

Table 4: Growth media used during laboratory work.

Medium	Composition
SMD/SMG (synthetic minimal dextrose/galactose, minimal medium)	0.17% Yeast nitrogen base (Difco) 0.5% Ammonium sulphate (Carl Roth GmbH) 2% D-glucose (SMD) or D-galactose (SMG) (PanReac AppliChem GmbH) amino acid mix (SERVA Electrophoresis GmbH), added to medium after autoclaving seperately: 80 mg/L Histidine 200 mg/L Leucine 320 mg/L Uracil 30 mg/L all other amino acids missing corresponding amino acid(s) for plasmid selection as necessary.
YPD (yeast peptone dextrose, full medium)	1% Bacto Yeast extract (BD) 2% Bacto-peptone (BD) 4% D-glucose (PanReac AppliChem GmbH)
YNB (yeast nitrogen base)	0.17% Yeast nitrogen base (Difco) 0.5% Ammonium sulphate (Carl Roth GmbH)
LB (lysogeny broth, full medium)	0.5% Bacto yeast extract (BD) 1% Bacto-tryptone (BD) 0.5% NaCl (Carl Roth GmbH)
Solid media for plates	addition of 2.2% agar (BD) for solid SMD plates, D-glucose and agar were autoclaved separately from YNB

2.4 Chemicals

The kits and chemicals used during research for this thesis are listed in Table 5.

Table 5: Chemicals used during laboratory work.

Chemicals	Company
6x DNA loading dye	Fermentas
Acrylamide	Carl Roth GmbH, Germany
APS (ammoniumperoxo-disulphate)	Fluka Chemie AG, Switzerland
Bromphenol blue	Carl Roth GmbH
BSA (bovine serum albumin)	Carl Roth GmbH, Germany
CAPS (N-cyclohexyl-3-aminopropanesulfonic acid)	Sigma-Aldrich
Chloroform	Carl Roth GmbH, Germany
Clarity western ECL substrate	Bio-Rad Laboratories GesmbH
DHE (dihydroethidium)	Sigma-Aldrich
DMSO (dimethyl sulfoxide)	Carl Roth GmbH, Germany
EDTA (ethylenediaminetetraacetic acid)	Carl Roth GmbH
GeneJET™ Plasmid Miniprep Kit	Thermo Fisher Scientific
GeneRuler™ 1 kb DNA Ladder	Thermo Fisher Scientific
Glycerine 87%	VWR
Glycine	Carl Roth GmbH, Germany
HCl (hydrochloric acid)	Carl Roth GmbH
HEPES (4-(2-hydroxyethyl)-1-piperazineethanesulfonic acid)	SERVA Electrophoresis GmbH
Isoamylalcohol	Merck KGaA, Germany
Isopropanol	Carl Roth GmbH, Germany
K_2HPO_4 (dipotassium hydrogenphosphate)	Carl Roth GmbH
KH_2PO_4 (potassium dihydrogen phosphate)	Carl Roth GmbH
Lithium acetate dihydrate	Sigma-Aldrich
Methanol	Carl Roth GmbH
Milk powder	Carl Roth GmbH, Germany
N,N'-Methylenebisacrylamide	Carl Roth GmbH, Germany
NaCl (natriumchlorid)	Carl Roth GmbH
NaOH (sodium hydroxide)	Carl Roth GmbH
PageRuler™ Prestained Protein Ladder	Thermo Fisher Scientific
Phenol	Carl Roth GmbH, Germany
PI (propidium iodide)	Carl Roth GmbH, Germany
Polyethylene glycol 400	Carl Roth GmbH, Germany
Quinacrine	Sigma-Aldrich

Rapamycin	Sigma-Aldrich
Restriction enzyme	New England Biolabs
SDS (sodium dodecyl sulfate)	SERVA Electrophoresis GmbH
Spermidine	Sigma-Aldrich
TEMED (N,N,N',N'-tetramethylethylendiamin)	Carl Roth GmbH, Germany
Tris (tris(hydroxymethyl)aminomethane)	Carl Roth GmbH
Triton X-100	Carl Roth GmbH
β-Mercaptoethanol	Carl Roth GmbH

2.5 Buffers and Solutions

The buffers and solutions used during research for this thesis are listed in Tables 6-11, sorted by method.

2.5.1 Cell Lysis, SDS-PAGE and Immunoblotting

Table 6: Buffers and solutions used for cell lysis, SDS-PAGE and immunoblotting.

Solution	Composition
Laemmli (lysis) buffer	0.3 g Bromphenol blue 100 mM β-Mercaptoethanol 10% Glycerine 2% SDS 50 mM Tris/HCl pH = 6.8 (no β-Mercaptoethanol for native conditions)
Electrophoresis buffer	192 mM Glycine 0.2% SDS 25 mM Tris/HCl pH = 8.8
Running gel	12.5% acrylamide 0.1% APS 0.4% N, N'-methylenbisacrylamide 0.2% SDS 0.01% TEMED

	250 mM Tris/HCl pH = 8.8 (no SDS for native blots)
Stacking gel	5% acrylamide 0.1% APS 0.13% N, N'-methylenbisacrylamide 0.2% SDS 0.01% TEMED 250 mM Tris/HCl pH = 6.8 (no SDS for native blots)
CAPS (blotting) buffer	10 mM CAPS 10% Methanol pH = 11
TBS buffer	150 mM NaCl 10 mM Tris/HCl pH = 7.4
TBS-T buffer	same as TBS, plus 0.02% Triton X-100
Blocking solution	3% milk powder or BSA (depending on following antibody solution) in TBS
Stripping buffer	100 mM β-Mercaptoethanol 2% SDS 62.5 mM Tris/HCl pH = 6.7

2.5.2 Antibodies

Table 7: Antibodies used for detection on membrane.

Antibody	Company
primary	
α-Synuclein	Sigma-Aldrich
Flag	Sigma-Aldrich
GAPDH	gift by Prof. Kohlwein
GFP	Roche, Mannheim

HA	Sigma-Aldrich
V5	Novex, Carlsbad
secondary	
α-mouse POD	Sigma-Aldrich
α-rabbit POD	Sigma-Aldrich

2.5.3 PI and DHE Staining

Table 8: Buffers and solutions used for PI and DHE staining.

Solution	Composition
PBS buffer	0.359% (w/v) K_2HPO_4 0.059% (w/v) KH_2PO_4 0.9% (w/v) NaCl pH = 7.2
PI solution	1:500 dilution in PBS
DHE solution	1:1000 dilution in PBS

2.5.4 Quinacrine/PI Staining

Table 9: Buffers and solutions used for quinacrine/PI staining.

Solution	Composition
Solution 1	0.1 M HEPES (pH = 7.6) YPD
Solution 2	0.1 M HEPES (pH = 7.6) 0.4 μM Quinacrine YPD
Solution 3	0.1 M HEPES (pH = 7.6) 2% Glucose ddH_2O
Solution 4	0.1 M HEPES (pH = 7.6) 2% Glucose PI, 1:500 dilution ddH_2O

2.5.5 Yeast Plasmid Isolation and Transformation

Table 10: Buffers and solutions used for *S. cerevisiae* plasmid miniprep and plasmid transformations.

Solution	Composition
Plasmid Isolation	
Yeast lysis buffer	1 mM EDTA 100 mM NaCl 1% SDS 2% (w/v) Triton X-100 10 mM Tris/HCl pH = 8
Phenol/chloroform/isoamylalcohol mix	25 : 24 : 1
Plasmid Transformation	
TE/LiAc	100 mM Lithium acetate 0.5 mM EDTA 5 mM Tris/HCl pH = 8
PEG solution	40% Polyethylene glycol 400 100 mM Lithium acetate 1 mM EDTA 10 mM Tris/HCl pH = 8
Carrier-DNA (ssDNA)	Carrier-DNA (ssDNA)

2.5.6 DNA Agarose Gel Electrophoresis

Table 11: Buffers and solutions used for DNA agarose gel electrophoresis.

Solution	Composition
TAE	40 mM Tris 1 mM EDTA pH = 8.0
Agarose gel	1% (w/v) Agarose in TAE 3 drops ethidium bromide

2.6 Software Used for Analysis

Microsoft Office for Mac 2016 (Excel, Word, PowerPoint) was used for data evaluation and presentation. Flow cytometry data was analysed using BD FACSDiva software. Quantificational analysis of immunoblots was performed using Image Lab version 5.2.1. Image editing was performed using ImageJ version 2-00-rc-49/1.51d[146]. Statistical analyses were done using SPSS version 23.

3. METHODS

3.1 Cell Biological Methods

3.1.1 Chronological Ageing

For ageing experiments overnight cultures (ONCs) were prepared by inoculation of 2 mL of corresponding SMD selection medium with a yeast colony and incubated at 28°C and 145 rpm for 16-20 hours. These ONCs were then used to inoculate 100 ml baffled flasks with 10-20 mL SMD medium to OD_{600} = 0.1. Strains were incubated at 28°C and 145 rpm until they reached OD_{600} = 0.3. Cells were then harvested for 5 minutes at 4000 rpm and 21°C. After centrifugation, cells were shifted to SMG medium for induction of LRRK2-GCK and LacZ expression and again incubated at 28°C and 145 rpm. This point in time was then used as point zero for the ageing.

3.1.2 Yeast Cell Storage

To store *S. cerevisiae* cells, 500 µL ONC were mixed with 500 µl 50% glycerine as a cryoprotectant and frozen at -80°C. When needed for inoculation, cells were streaked on YPD or SMD selection plates and incubated for two days at 28°C. Plates with colonies were stored at 4°C for up to 14 days.

3.1.3 DHE and PI Staining for Flow Cytometry

In order to analyse cell death propidium iodide (PI), a fluorescent agent that stains cells with ruptured membranes, was used. Cell samples of 35 µL were collected in 96-well plates and centrifuged for 5 minutes at 21°C and 4000 rpm. Cells were resuspended in 250 µL PI solution and incubated in the dark for 10 minutes. For analysis of oxidative cell stress, the superoxide indicator dihydroethidium (DHE) was used. For this set up, cells were instead resuspended in 250 µL DHE solution and incubated in the dark for 5 minutes. After staining, centrifugation was repeated. Cells were resuspended in 250 µL PBS and then analysed via flow cytometry. For each measurement 30000 cells were evaluated.

3.1.4 Induction of Autophagy by Treatment with Rapamycin, Spermidine or Calcium

Rapamycin, spermidine and calcium were used to induce autophagy during the ageing. Cells were exposed to the substances with the shift to galactose media, concurrent with the induction of LRRK2 and LacZ expression. To achieve this, the agents were mixed into the SMG media prior to the shift. The substance concentrations for the initial experiments were chosen based on previous experience our work group obtained when working with an αSyn yeast model. For the initial experiments, the control consisted of cells without added substance. For further experiments with rapamycin treatment, DMSO was added to the control, as DMSO was used to solve rapamycin and has itself been reported to affect yeast cell growth[147,148]. In small doses, it has been shown to be beneficial to cell proliferation. As DMSO is toxic at higher doses, it was ensured that concentrations did not exceed 0.1% (v/v). Where more than one concentration of rapamycin was observed, dillution was chosen in such a way that an equal amount of DMSO was added to all cultures.

3.1.5 Clonogenic Cell Survival Assay

Clonogenic survival of the chronologically ageing yeast cultures under treatment with rapamycin was determined via survival plating. 30 or 35 µL of a 1:10000 dilution of the main culture in ddH2O were plated onto YPD agar. Plates were then incubated at 28°C for 3 days and colonies counted using an Olli MBS cell counter. In order to calculate how many cells had been plated, cell density of the cell cultures was measured using a CASY cell counter system. Cultures were diluted 1:10000 in Casyton. Two separate measurement cycles were performed for each sample. Survival was defined by how many of the plated cells (dead or alive) were able to grow colonies.

3.1.6 Fluorescence Microscopy

3.1.6.1 Monitoring Protein Localisation

In order to visually monitor autophagy, cells containing endogenously GFP-tagged Atg8, a protein located in the autophagosomal membrane, were studied. To observe αSyn localisation in the presence of LRRK2, cells expressing EGFP-tagged αSyn via a pUG23 vector were used. In each case 200 µL cells were harvested, directly dosed with 2.5 µg/mL PI and incubated in the dark for 5 minutes. Samples were washed in 500 µL PBS directly prior to analysis under the fluorescence microscope. GFP fluorescence was detected using an eGFP filter, PI

fluorescence using a dsRED filter. Exposure time varied as necessary but was kept constant for all clones per time value.

3.1.6.2 Monitoring Cell Acidity

Quinacrine is a fluorescent dye that accumulates in acidic compartments and can thus be used to monitor cell acidity. To accomplish this, 250 µL cells were harvested and washed in Solution 1, followed by quinacrine staining in Solution 2 for 10 minutes at 28°C and 145 rpm. Keeping cells on 4°C for the rest of the experiment, they were then washed twice with Solution 3, followed by PI staining in Solution 4, incubating in the dark for 10 minutes. Samples were then analysed under the fluorescence microscope. Quinacrine fluorescence was detected using an eGFP filter, PI fluorescence using a dsRED filter. Exposure time varied as necessary but was kept constant for all clones per time value.

3.2 Biochemical methods

3.2.1 Cell Lysis

Cell lysis was needed to isolate proteins for further SDS-PAGE and immunoblot analysis. Samples of OD_{600} = 3 (OD_{600} = 8 for aggregate blots) were harvested, suspended in 200 µL NaOH (0.1M) and incubated in a thermomixer for 5 minutes at 21°C and 1400 rpm. After 5 minutes of centrifugation at 21°C and 4000 rpm, the pellet was resuspended in 150 µL Laemmli buffer and incubated in a thermomixer under the previous conditions. After another round of centrifugation, 100 µL of the supernatant were transferred into new reaction tubes to avoid accidental transferal of the pellets onto gels. Samples were then either directly used for SDS-PAGE or stored at 4°C.

3.2.2 SDS-PAGE and Immunoblotting

SDS-PAGE with consecutive immunoblotting was used to assess an array of protein expression-related questions. Expression of LRRK2 and LacZ was checked via the V5-tag under regular conditions and under exposure to rapamycin. Expression control and quantification of the endogenously HA-tagged Pep4 was done using the HA-tag, expression control of Pep4 overexpressed via pESC-HIS using the FLAG-tag. For αSyn^{EGFP}, expression was checked via the GFP-tag and aggregates were detected with an αSyn specific antibody on native blots. To determine vacuolar degradation of endogenously GFP-tagged Atg8 as a measure of autophagic

flux, GFP-Atg8 and free GFP were detected using Anti-GFP antibody. The housekeeping protein GAPDH was used as a loading control for all setups.

Cell lysates were separated at 200 V on a 12.5 % SDS-polyacrylamide gel and then electroblotted to a PVDF membrane using CAPS buffer for 75 minutes at 220 mA and room temperature. Samples for native aggregate blots were separated on 10% polyacrymide gels, with gels and blots run at 4°C.

To avoid unspecific binding, membranes were blocked under shaking conditions for at least 1 hour with 3% milk powder or 3% BSA in TBS (depending on the following antibody solution). This was followed by incubation with a primary antibody at room temperature for 1-3 hours or at 4°C overnight. After washing the membranes with TBS-T for 15 minutes, they were incubated with the respective peroxidase-conjugated affinity-purified secondary antibody for at least 1 hour. Following extensive washing with TBS-T, the reaction was developed by enhanced chemiluminescent staining using ECL substrate and detected via ChemiDoc™ Touch.

3.2.3 Stripping

Immunoblot membranes were stripped where it was necessary to use an antibody for detection of proteins overlapping with another antibody already bound to the membrane. Membranes were incubated in stripping buffer at 60°C for 15 minutes and then washed with TBS-T until no more β-mercaptoethanol could be nasally detected. At this point blocking and antibody incubation was repeated as described above.

3.3 Molecular Biological Methods

3.3.1 Yeast Plasmid Transformation

The pYES2/CT plasmid set for LRRK2 expression and control (see above) was transformed into BY4741 wild type and into BY4741 harbouring endogenously tagged GFP-Atg8. pESC-HIS for Pep4 expression, pUG23 for αSyn^{EGFP} expression and their respective empty control vectors were introduced into the BY4741 wild type in a double plasmid transformation with the pYES2/CT set.

ONCs of 5-10 mL were used to inoculate 50 mL of YPD (wild type) or SMD (selection) media to an OD_{600} = 0.2. Cells were then grown to OD_{600} =0.6-0.8, harvested and washed with 10 mL ddH_2O, the centrifugation performed for 5 minutes at 4000 rpm and 21°C. Cells were washed with 10 mL TE/LiAc under the same conditions and then resuspended in 300-500 µL

TE/LiAc and incubated at 28°C and 145 rpm for 30 minutes. Meanwhile ss-DNA was first heated at 95°C for 10 minutes and then put on ice for at least 10 minutes. Once incubation was finished, 50 µL of the cell solution were mixed with 300 µL PEG solution, 5 µL ss-DNA and 0.5-1 µg plasmid DNA. After thorough vortexing, the suspension was again incubated for 30 minutes at 28°C and 145 rpm. Cells were then heat shocked at 42°C for 20 minutes. After centrifugation at 13000 rpm for 12 seconds, the supernatant was removed and the pellet resuspended in 70 µL ddH_2O. The cell solution was then plated onto selection plates and incubated at 28°C for 2 days. Average-sized clones were then picked and streaked onto new selection plates. After 2 further days of incubation at 28°C the clones were used to inoculate ONCs for ageings and cryostorage.

3.3.2 Yeast Plasmid Isolation

In order to isolate needed pUG23 plasmids from yeast cells, 5 mL ONCs were harvested for 5 minutes at 4000 rpm and 21°C and resuspended in 300 µL yeast lysis buffer. About 300 mg glass beads and 200 µL phenol/chloroform/isoamylalcohol mix were added. After vortexing for 3 minutes, samples were centrifuged for 10 minutes at 10000 rpm and 21°C. The water phase was transferred into a new reaction tube and 150 µL isopropanol were added to precipitate the DNA. Samples were centrifuged for 10 minutes. Pellets were then washed twice soaking in 750 µL ethanol for 2 minutes, followed by 2 minute centrifugation at 10000 rpm and 21°C. After air drying pellets were resuspended in ddH_2O. The concentration of isolated DNA was checked via NanoDrop.

3.3.3 Restriction Digest and Agarose Gel Electrophoresis

In order to check the isolated pUG23 plasmids, correct plasmid size was confirmed via agarose gel electrophoresis. To accomplish this, plasmids were first linearised by restriction digest with the restriction enzyme XBaI. The digest was performed with 1 µg of plasmid DNA, 1 µL enzyme and 1x NEBuffer in a total reaction volume of 50 µL at 37°C for one hour. The restriction enzyme was then inactivated by incubation at 65°C for 20 minutes. The size of pUG23 plasmids with and without αSyn was confirmed by separation on a 1% agarose gel and comparison to DNA ladder standard.

3.3.4 *E. coli* Plasmid Transformation

Transformation of pU23 plasmids into *E. coli* cells via electroporation was performed in order to amplify plasmids for later transformation into *S. cerevisiae*. Cuvettes were sterilised under UV light for 10 minutes and then precooled on ice. For electroporation, 100-150 ng of plasmid DNA and 40 µL of competent *E. coli* cells were mixed in cuvettes and shocked at 2500 V. After adding 1 mL of LB media, cells were incubated at 37°C for 30 minutes. Cells were then plated onto LB agar plates (containing 100 µg/mL ampicillin for selection) and incubated at 37°C overnight.

3.3.5 *E. coli* Plasmid Isolation

Plasmid isolation from *E. coli* was performed using the "GeneJET™ Plasmid Miniprep Kit" by Thermo Fisher Scientific following the provided instructions. The concentration of isolated plasmids was checked via NanoDrop.

3.4 Statistics

A one-way ANOVA followed by a Bonferroni post-hoc test was used to calculate P-values. For diagrams spanning several days, a two-way ANOVA with time and strain as independent factors followed by a Bonferroni post-hoc test was used. Error bars showing ± S.E.M. are included in shown diagrams. The number of independent data points (n) is indicated in the figure legends of the corresponding graphs.

4. Results

4.1 LRRK2 Causes a Block of Autophagy

To confirm whether or not LRRK2 affects autophagy in our *S. cerevisiae* model, we employed methods of Atg8 detection and quantification (for measure of non-specific autophagy) as described by Klionsky et al.[149]. Atg8 is a ubiquitin-like protein involved in autophagosome formation and cargo recruitment[150]. It undergoes conjugation to PE on the autophagosomal membrane and is widely used as a marker for autophagosomes. For experimental purposes, Atg8 can be tagged with GFP at the N-terminus (as the C-terminus is cleaved off by Atg4 in processing). This allows for rudimentary tracking of autophagosomes and their vacuolar fusion under the fluorescence microscope. If autophagosomes do fuse with the vacuole, Atg8 is degraded while the free GFP remains relatively resistant to hydrolysis and can be detected in cell lysates. The amount of free GFP and GFP bound to Atg8 can be checked and compared via immunoblotting and used as an indicator for autophagic flux.

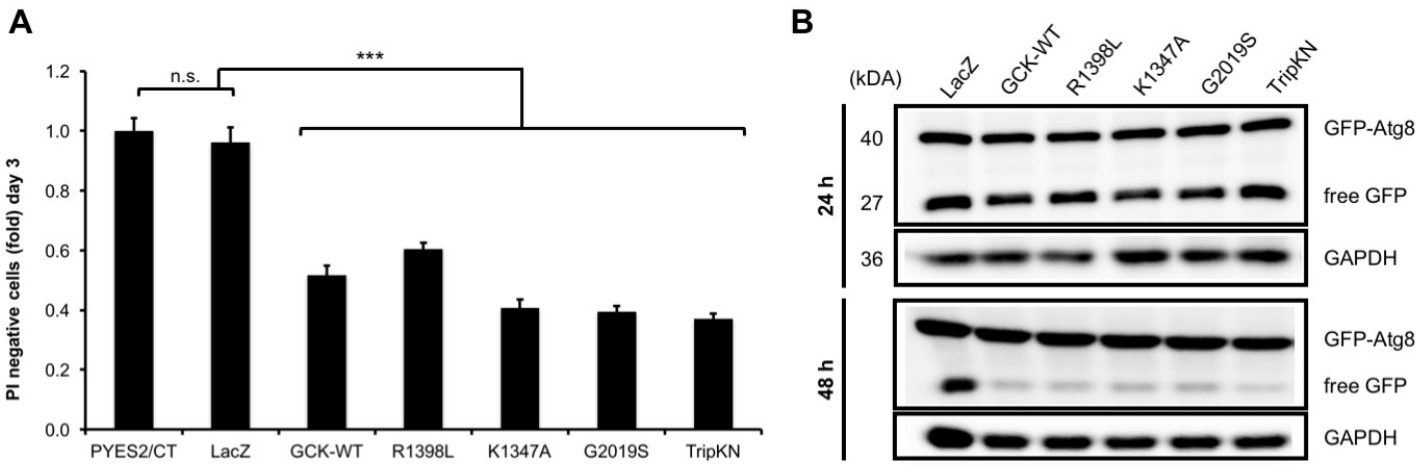

Figure 5: The influence of LRRK2 toxicity on autophagy measured by immunoblotting the autophagosomal membrane protein GFP-Atg8. Endogenously GFP-tagged Atg8 yeast cells heterologously expressing human LRRK2-GCK in its wild type form (GCK-WT) and several mutant alleles (R1398L, K1347A, G2019S, TripKN) compared to cells expressing LacZ or the empty vector. (**A**) Flow cytometric quantification of PI stained cells as a signifier of cell death on day 3. Mean ± S.E.M., , $n = 4$, *** = $P < 0.001$, n.s. = not significant. (**B**) Immunoblot analysis of GFP-Atg8 and free GFP as a measure of autophagic flux 24 hours and 48 hours into the ageing. GAPDH was detected as a loading control.

We analysed the autophagic flux in cells expressing the LRRK2 wild type and the four mutants described above, and compared them to the controls throughout the chronological ageing. The experiments were carried out at four chosen time points: 24 hours, 40 hours, 48 hours and 72 hours after induction of LRRK2 expression. Flow cytometry was used to confirm that LRRK2-related cell death at 72 hours occurred as to be expected for this model (Figure 5A).

Fluorescence microscopy revealed an apparent block of autophagy on day 2 (Figure 7). On day 1 there was no observable difference between LRRK2 expressing cells and the control. At 40 hours however, collections of green fluorescent dots – presumably autophagosomes – started to accumulate in LRRK2 expressing cells. This effect grew slightly more pronounced at 48 hours. At 72 hours after LRRK2 induction, increased cell death made it difficult to visually evaluate the micrographs. Quantification analysis however revealed that the phenotypes of LRRK2 and the control were restored in their similarity, albeit LRRK2 still had a significantly increased count of cells harbouring two or more autophagosomes (Figure 6). Overall, the quantification underscored the observed effect, with the vacuolar signal decreasing and autophagosome accumulation rising for LRRK2 on day 2. There was no difference between the LRRK2 wild type and any of the mutant alleles (Figure 7B) or the LacZ control and the empty vector (data not shown). The block of autophagy could be confirmed via immunoblot in cooperation with Andreas Aufschnaiter (Figure 5B).

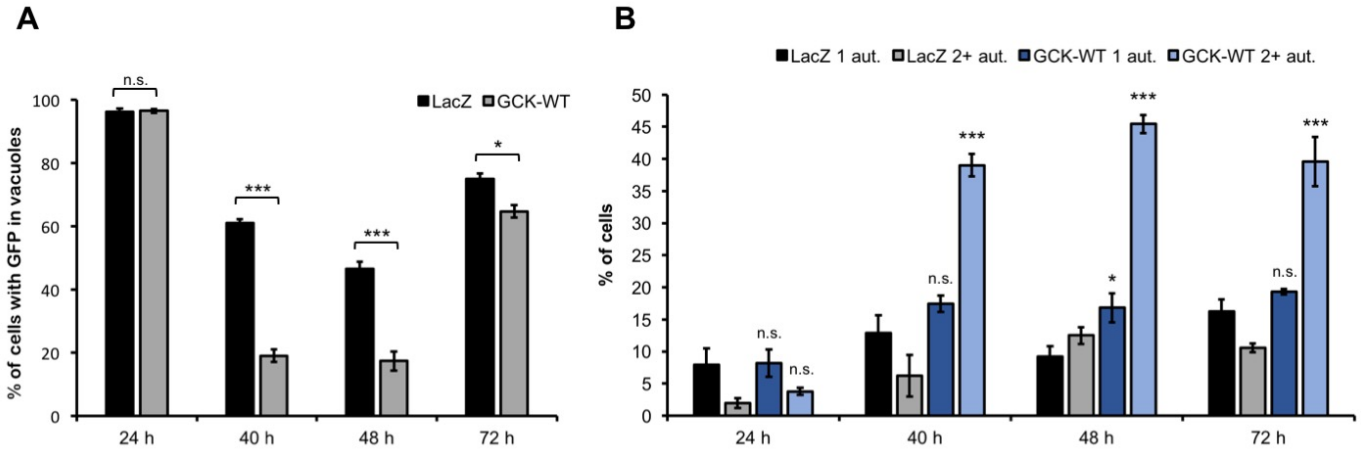

Figure 6: The influence of LRRK2 toxicity on autophagy analysed through the autophagosomal membrane protein GFP-Atg8. Quantification of fluorescent micrographs of endogenously GFP-tagged Atg8 yeast cells heterologously expressing human LRRK2 or the LacZ control. Micrographs were taken at 24, 40, 48 and 72 hours into the ageing. Dead cells were excluded from analysis via PI staining. Mean ± S.E.M., , n = 3-4, *** = $P < 0.001$, * = $P < 0.05$, n.s. = not significant compared to the corresponding LacZ value. (**A**) Percentage of cells with fluorescent vacuoles. (**B**) Percentage of cells featuring one autophagosome (1 aut.) or two or more autophagosomes (2+ aut).

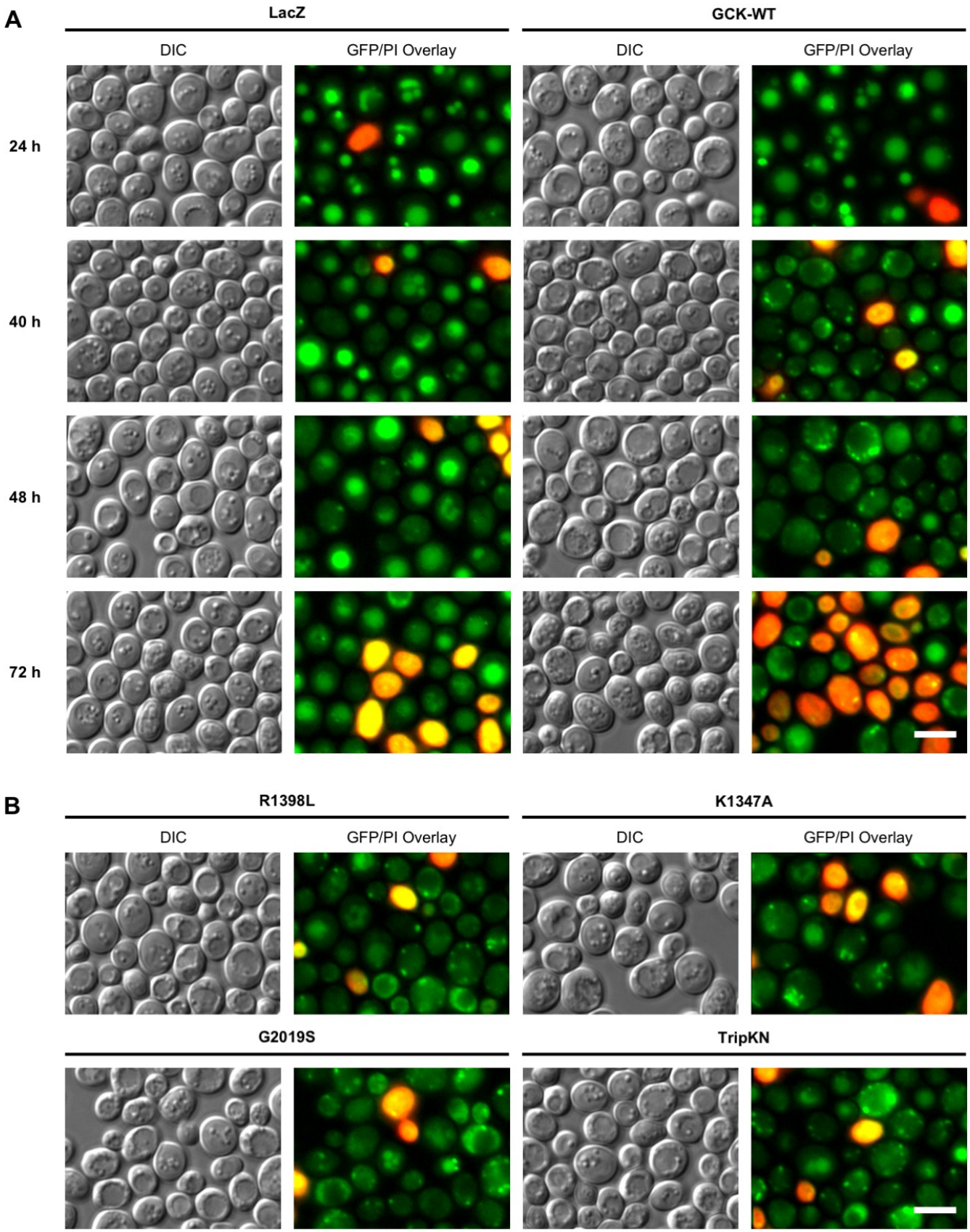

Figure 7: The influence of LRRK2 toxicity on autophagy visualised through the autophagosomal membrane protein GFP-Atg8. Differential interference contrast (DIC) and fluorescent microscope analysis of PI stained, endogenously GFP-tagged Atg8 yeast cells heterologously expressing human LRRK2. Scale bar represents 5 μm. (**A**) LRRK2-GCK in its wild type form (GCK-WT) compared to cells expressing LacZ. Representative micrographs were taken at 24, 40, 48 and 72 hours after induction of LRRK2-GCK expression. (**B**) Micrographs show cells carrying LRRK2 mutants (R1398L, K1347A, G2019S, TripKN) at 48 hours.

4.2 Induction of Autophagy Via Rapamycin Reduces LRRK2 Toxicity

As shown above, the expression of LRRK2 in yeast leads to increased cell death, correlating with a block of autophagy. Considering this, a new question was posed: Could an upregulation of autophagy reduce the LRRK2-associated cell death? We explored this using several autophagy-inducing substances: Spermidine, calcium and rapamycin. To analyse the effect of these agents on our model, we compared the viability of cells expressing the GCK-WT fragment to the controls throughout 7 day ageings.

4.2.1 Exposure to Spermidine Does Not Reduce Cell Death Caused by LRRK2

Spermidine has been shown to induce autophagy in several model organisms, including yeast[151]. This is thought to be due to the inhibition of histone acetyl transferases by spermidine, leading to a reduced acetylation of histone H3. The epigenetic changes caused by this then result in an increased expression of autophagy-related genes.

The viability of both, LRRK2-expressing cells and the LacZ control was decreased when exposed to 4 mM spermidine (Figure 8A). Notably, oxidative cell stress was significantly increased for all cells under spermidine treatment (Figure 8B).

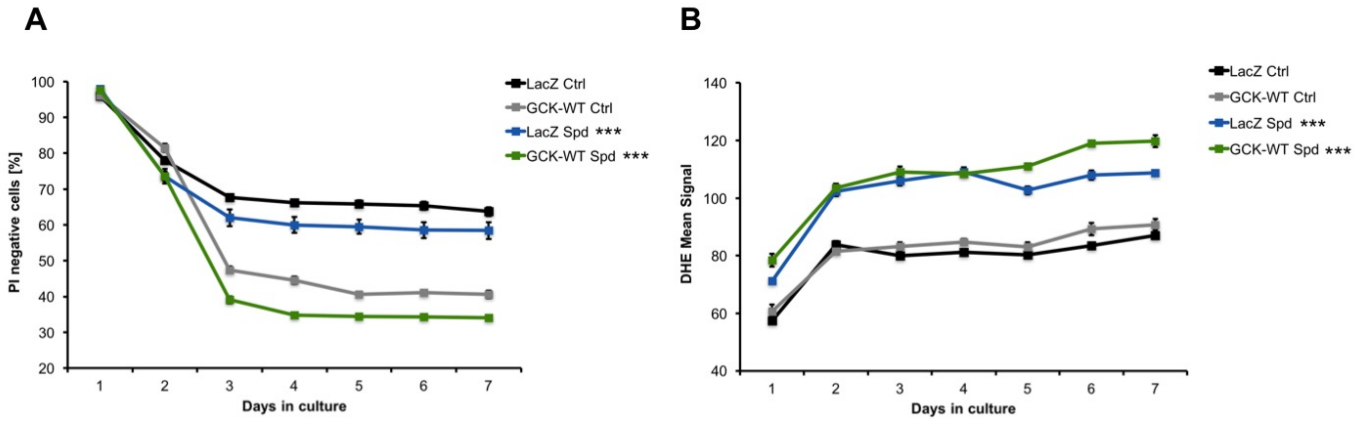

Figure 8: Spermidine does not reduce LRRK2 toxicity. Yeast cells heterologously expressing human LRRK2-GCK in its wild type form (GCK-WT) or expressing the LacZ control were exposed to 4 mM spermidine (Spd) and compared to a control set (Ctrl) without spermidine. Mean ± S.E.M., *** = $P < 0.001$, $n = 4$. (**A**) Flow cytometric quantification of PI stained cells as a signifier of cell death over 7 days. (**B**) Flow cytometric quantification of DHE stained cells as a signifier of oxidative cell stress over 7 days.

4.2.2 Exposure to Calcium Does Not Reduce Cell Death Caused by LRRK2

Calcium's influence on autophagy regulation is well established, although the exact mechanisms involved are as of yet unclear[152]. Calcium homeostasis has also been shown to have an important impact on the toxicity of αSyn[153]. Experimental data from our group have already shown that the administration of calcium induces autophagy and alleviates αSyn toxicity in yeast (Habernig et al., unpublished).

In our LRRK2 model, neither of the tested calcium concentrations (2 mM and 25 mM) led to a decrease of LRRK2-related cell death (Figure 9A). Additionally, there was no significant difference in oxidative cell death between cells exposed to calcium and the control (Figure 9B).

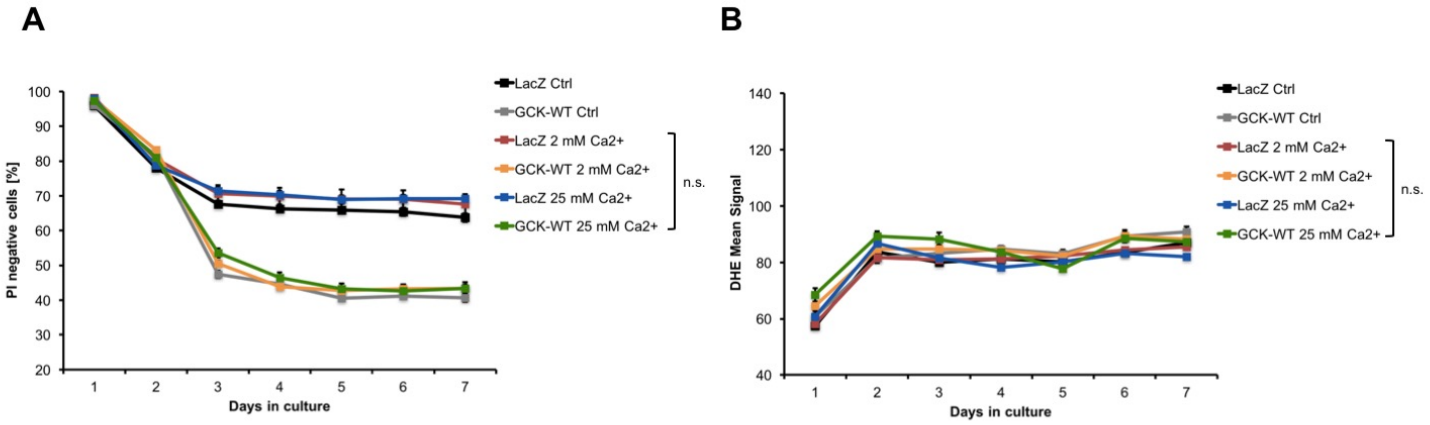

Figure 9: Calcium does not reduce LRRK2 toxicity. Yeast cells heterologously expressing human LRRK2-GCK in its wild type form (GCK-WT) or expressing the LacZ control were exposed to 2 mM or 25 mM calcium (Ca2+) and compared to a control set (Ctrl) with no added calcium. Mean ± S.E.M., $n = 4$, n.s. = not significant compared to the relating control value. (**A**) Flow cytometric quantification of PI stained cells as a signifier of cell death over 7 days. (**B**) Flow cytometric quantification of DHE stained cells as a signifier of oxidative cell stress over 7 days.

4.2.3 Exposure to Rapamycin Reduces Cell Death Caused by LRRK2

As suggested by its name, rapamycin's interaction partner within the cell is the Target Of Rapamycin (TOR) kinase. TOR is a primary integrator of nutrient-derived signals in eukaryotic cells[129,131] and represses autophagy when nutrients are available[130]. Rapamycin inhibits TOR activity, which results in an upregulation of autophagy.

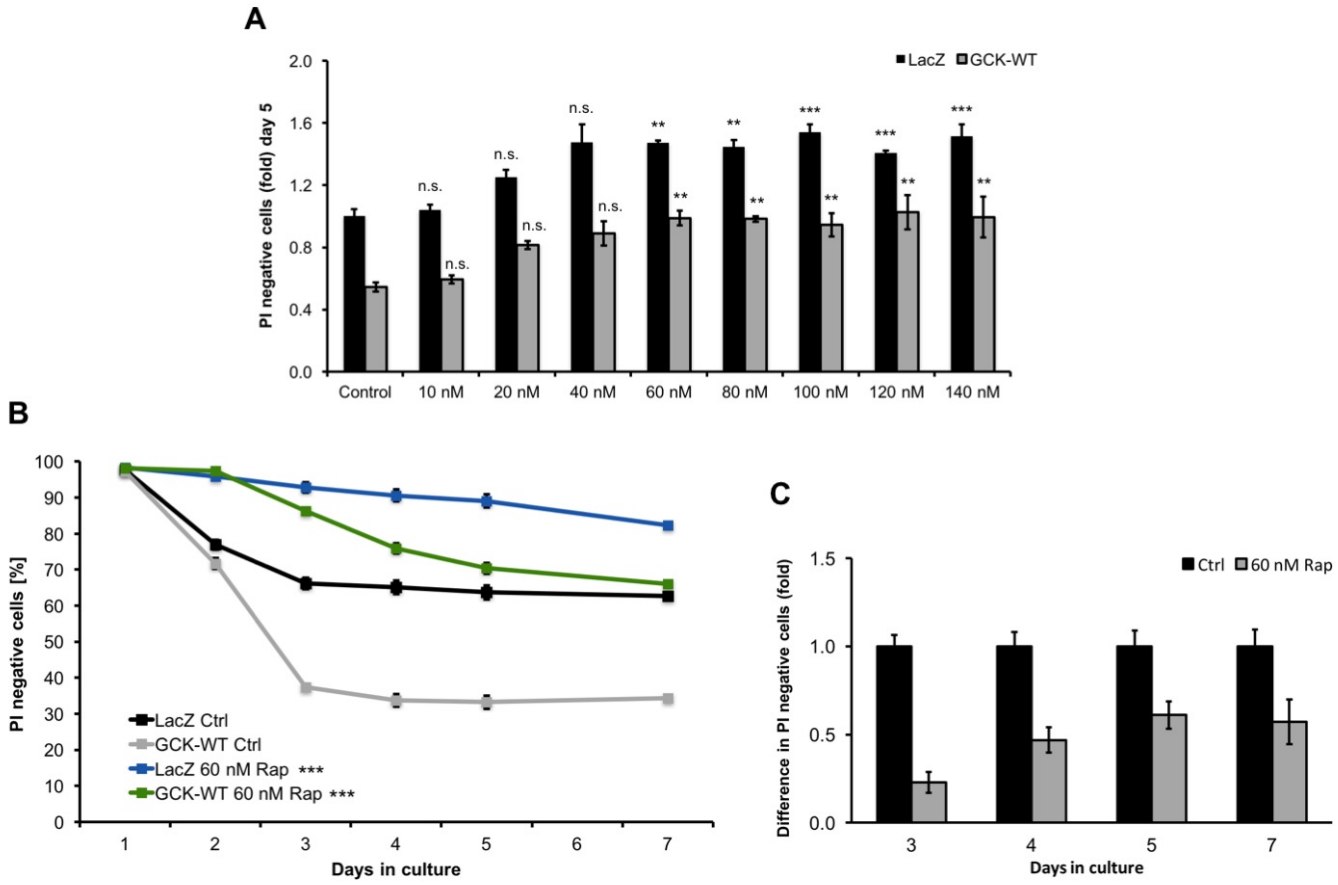

Figure 10: Rapamycin reduces LRRK2 toxicity. Yeast cells heterologously expressing human LRRK2-GCK in its wild type form (GCK-WT) or expressing the LacZ control were exposed rapamycin (Rap) and compared to a control set (Ctrl) exposed to the corresponding amount of DMSO. Flow cytometric quantification of PI stained cells as a signifier of cell death. Mean ± S.E.M., $n = 4$, *** = $P < 0.001$, ** = $P < 0.01$, n.s. = not significant compared to the relating control value. (**A**) Flow cytometric quantification of cells exposed to 10, 20, 40, 60, 80, 100, 120 and 140 nM rapamycin on day 5 to determine optimal concentration. (**B**) Flow cytometric quantification of cells eposed to 60 nM rapamycin over 7 days. (**C**) Difference in viability between LacZ expressing cells and LRRK2 expressing cells exposed to rapamycin (60 nM Rap) compared to viability difference between the LacZ expressing cells and LRRK2 expressing cells exposed to DMSO (Ctrl); data taken from (**B**).

4.2.3.1 Determination of Optimal Rapamycin Concentration

As preliminary results using 6 nM rapamycin showed a small but promising effect, we first set out to the determine the optimal rapamycin concentration to work with. To this end the viablity of cells exposed to 10, 20, 40, 60, 80, 100, 120 and 140 nM rapamycin were compared (Figure 10A). While viability rose with concentration at the lower end, this effect was not present for concentrations higher than 60 nM. Additionally, standard deviations were increased at concentrations higher than 80 nM. A concentration of 60 nM rapamycin was chosen as optimal for further ageings (for a timeline of cell viability under treatment with 60 nM rapamycin throughout the ageing, consult Figure 10B). It is important to note that rapamycin did not merely decrease cell death for all cells, but lessened LRRK2 toxicity in particular. The difference between LacZ expressing cells treated with rapamycin and the control was significantly higher than the difference for LRRK2 expressing cells (Figure 10C).

4.2.3.2 Rapamycin Increases Clonogenic Survival of Cells Expressing LRRK2

To determine how rapamycin affects proliferation in our model, we performed a clonogenic survival assay. Survival was markedly increased for cells exposed to rapamycin (Figure 11). Furthermore, while the difference in survival between LacZ and LRRK2 expressing cells of the control remained substantial, there was no significant difference in survival between LacZ and LRRK2 expressing cells under treatment with rapamycin.

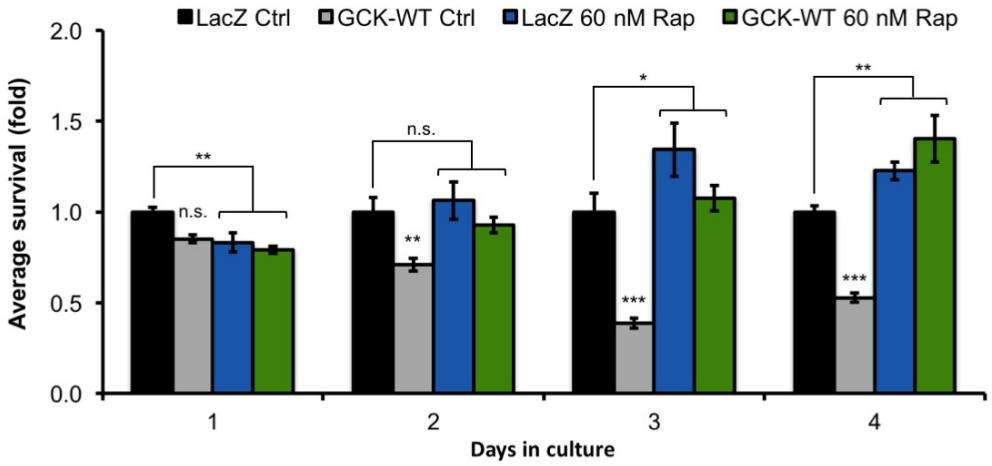

Figure 11: Rapamycin increaes the clonogenic survival of cells expressing LRRK2. Yeast cells heterologously expressing human LRRK2-GCK in its wild type form (GCK-WT), expressing the LacZ control or harbouring the empty vector under exposure to 60 nM rapamycin compared to a DMSO control over a period of 4 days. LacZ and GCK-WT exposed to Rapamycin never differed significantly from each other. Mean ± S.E.M., n = 4-8, *** = $P < 0.001$, ** = $P < 0.01$, * = $P < 0.05$, n.s. = not significant compared to the relating control value.

4.2.3.3 Rapamycin Does Not Delay Cell Growth in Our Model

Rapamycin has been shown to slow down cell growth[129]. If this effect was significantly in play for our setup, it would compromise the comparability with the control set. To ensure that this was not the case for our chosen concentration, we analysed cell count and cell size during the exponential growth phase, 16 hours into the ageing. Neither cell count nor size differed significantly between cells treated with rapamycin and the control (Figure 12A and B).

4.2.3.4 Rapamycin Does Not Change The Level of LRRK2 Expression

To test whether the rescuing effects of rapamycin were a result of a reduced LRRK2 expression, we performed immunoblot analysis. There was no significant difference for expression levels of either LRRK2 or the LacZ control under exposure to rapamycin (Figure 12C and D).

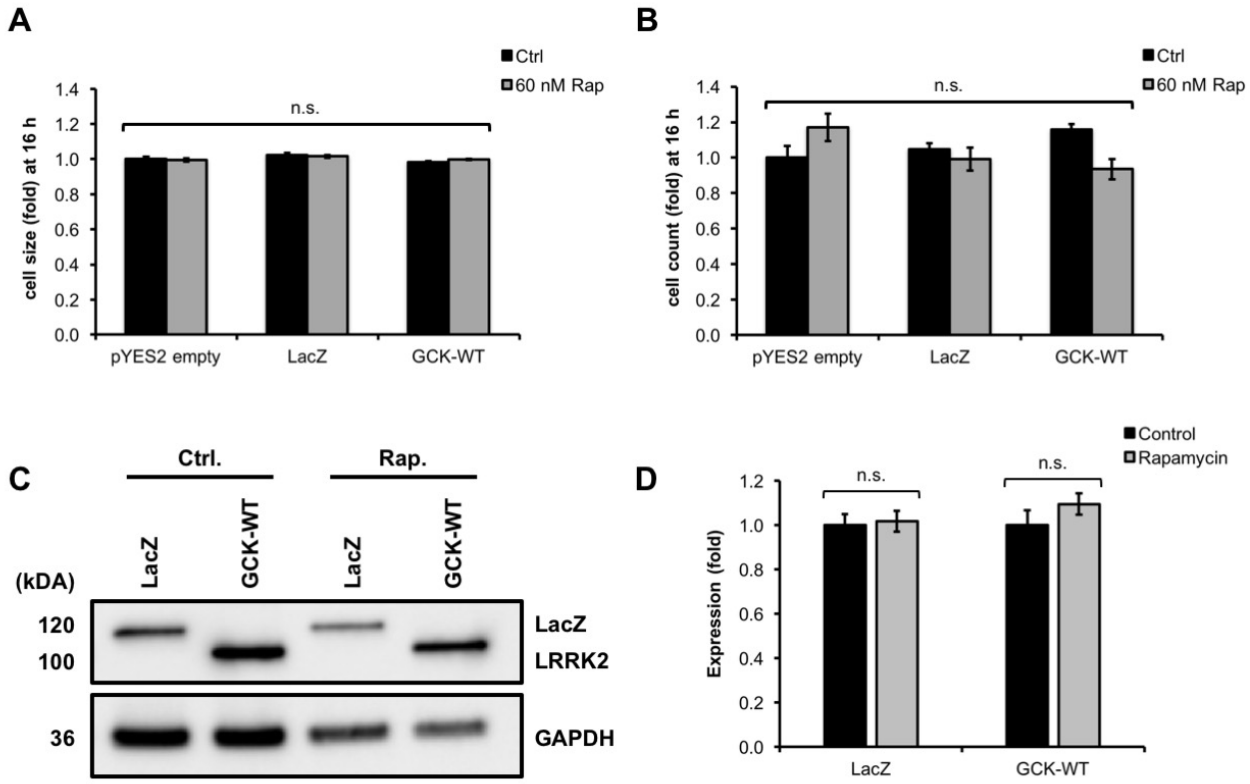

Figure 12: Rapamycin does not delay cell growth or affect LRRK2 expression levels in our model. Yeast cells heterologously expressing human LRRK2-GCK in its wild type form (GCK-WT), expressing the LacZ control or harbouring the empty vector under exposure to 60 nM rapamycin compared to a control without rapamycin. Cell size (**A**) and cell count (**B**) were measured using a CASY cell counter system 16 hours into the ageing. Mean ± S.E.M., $n = 8$, n.s. = not significant. (**C**) Immunoblot of LRRK2 and LacZ expression. The blot was probed with antibodies directed against the V5 epitope to detect the V5-tagged LacZ and LRRK2-GCK and against GAPDH as a loading control. (**D**) Quantification of expression levels with data obtained from (C). Mean ± S.E.M., $n = 4$, n.s. = not significant.

4.2.3.5 Calcium Treatment Does Not Affect Alleviation of Cell Death by Rapamycin

We exposed cells to a combined treatment with rapamycin and calcium, to investigate whether we could further reduce cell death in this manner. There was no synergistic effect – the viability of cells under rapamycin treatment remained the same whether or not calcium was added (Figure 13).

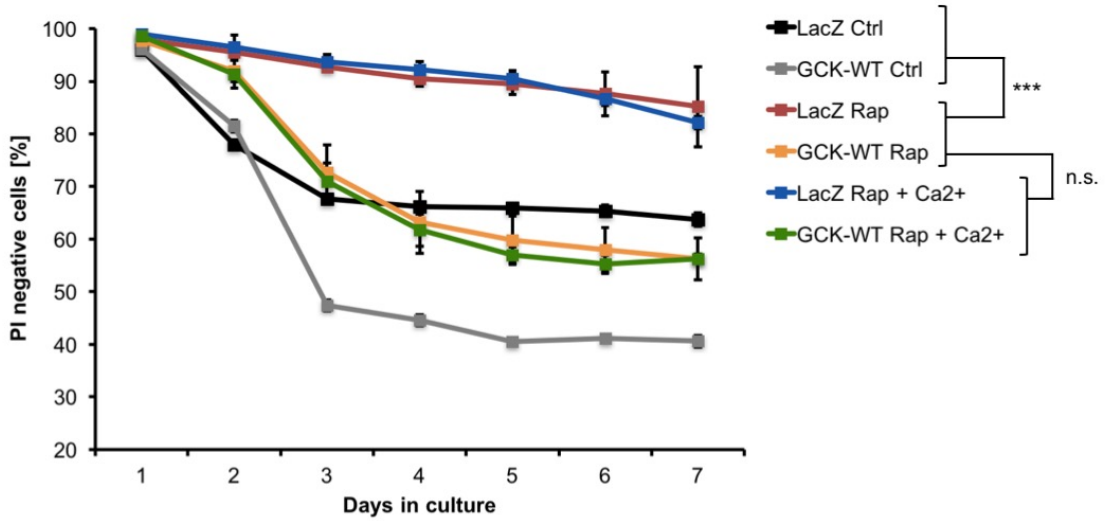

Figure 13: Calcium treatment does not affect the alleviation of cell death by rapamycin. Yeast cells heterologously expressing human LRRK2-GCK in its wild type form (GCK-WT) or LacZ under exposure to 60 nM rapamycin (Rap) compared to a combined treatment of 60 nM rapamycin and 2 mM Calcium (Ca2+) and to a DMSO control. Flow cytometric quantification of PI stained cells as a signifier of cell death over 7 days. Mean ± S.E.M., $n = 4$, *** = $P < 0.001$, n.s. = not significant.

4.3 LRRK2 Has No Effect on Cell Acidity

Maintenance of pH homeostasis within the cell and its different compartments is crucial to biological function. Many processes, including autophagy, require proper cellular pH maintenance – for example, compromising vacuolar acidification allows for the initial steps of autophagy to proceed but inhibits fusion of the autophagosome with the vacuole, leading to an accumulation of autophagosomes[127].

Our group has previously shown that αSyn causes cytosolic acidification in yeast[143]. To examine whether a change in cellular pH could be involved in LRRK2 toxicity as well, we analysed our ageing model for changes in cellular pH. Cells were stained with quinacrine – a fluorescent dye that accumulates in acidic cellular compartments – and analysed via fluorescence microscopy. This was done on day 1 of the ageing, when effects should already be observable but the naturally occurring age-related yeast acidification is not yet too prominent to render analysis impossible. Micrographs showed no visual difference between the controls and cells expressing any of the LRRK2 variants (Figure 15A). To confirm this, cells with acidic cytosol were counted for cells expressing the GCK wild type and the controls. There was no significant difference in cytosolic acidification (Figure 15B). LRRK2-related cell death on day 3 was confirmed via flow cytometry (Figure 14).

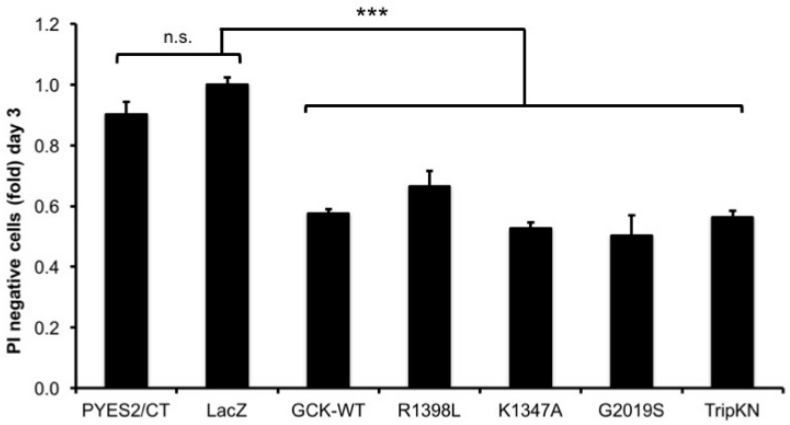

Figure 14: LRRK2 induced cell death occurs on day 3 of the ageing. Flow cytometric quantification of PI stained cells as a signifier of cell death for yeast heterologously expressing human LRRK2-GCK in its wild type form (GCK-WT) and several mutant alleles (R1398L, K1347A, G2019S, TripKN) compared to cells expressing LacZ or harbouring the empty vector. Mean ± S.E.M., , $n = 4$, *** = $P < 0.001$, n.s. = not significant.

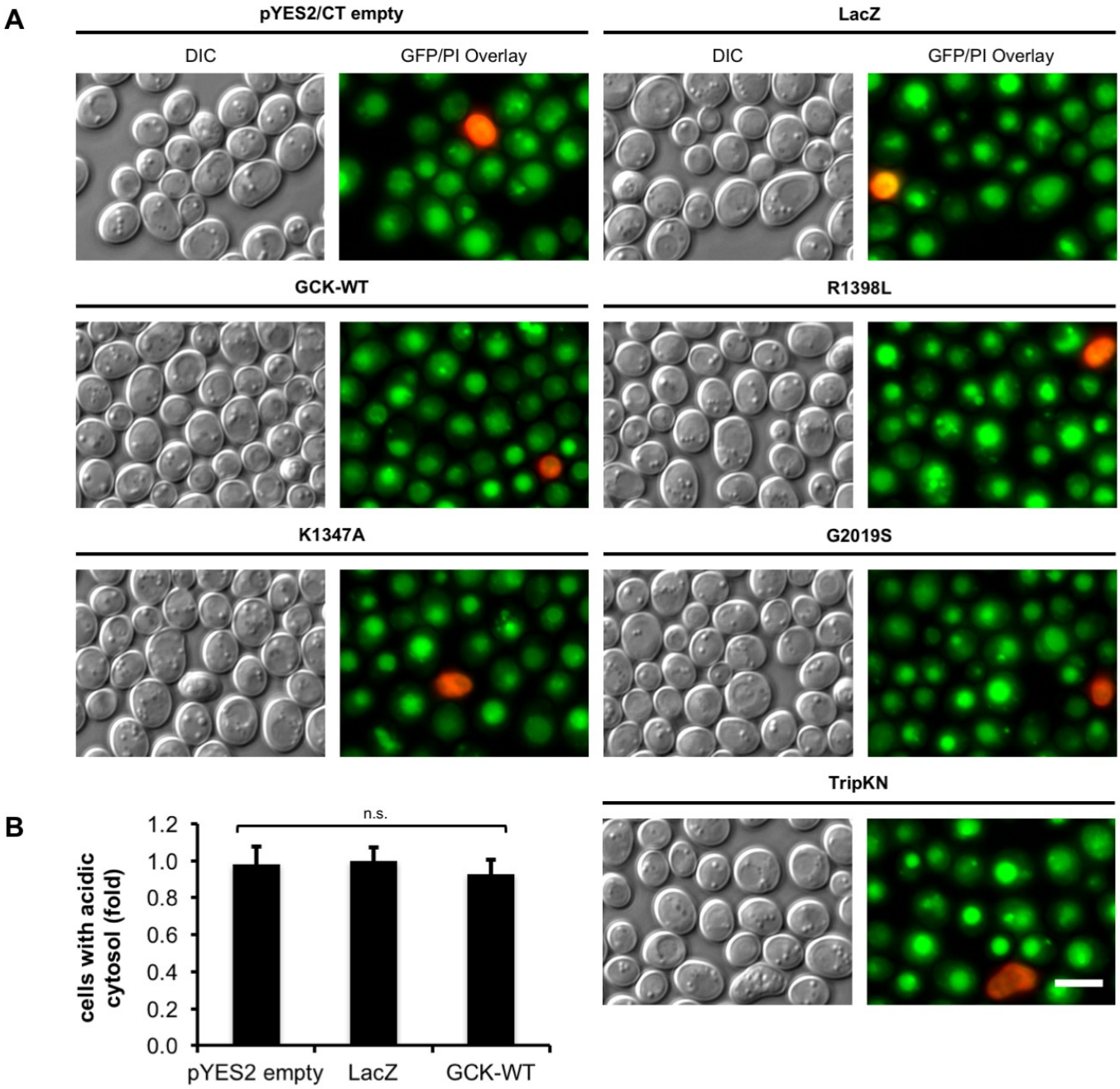

Figure 15: LRRK2 toxicity does not affect cell acidity. (**A**) Differential interference contrast (DIC) and fluorescent microscopy analysis of yeast cells heterologously expressing human LRRK2-GCK in its wild type form (GCK-WT) and several mutant alleles (R1398L, K1347A, G2019S, TripKN) compared to cells expressing LacZ or harbouring the empty vector. Cells were stained with quinacrine to visualise acidic cell organelles and PI to account for cell death. Micrographs were taken at 24 hours after induction of LRRK2 expression. Scale bar represents 5 μm. (**B**) Quantification of cells with acidic cytosol counted using micrographs taken in (**A**), comparing cells expressing LRRK2-GCK wild type to the LacZ and empty vector controls. Mean ± S.E.M., $n \geq 198$, n.s. = not significant.

4.4 Pep4 Overexpression Reduces LRRK2 Toxicity

Pep4 is an important vacuolar aspartyl protease. Its lysosomal mammalian orthologue cathepsin D (CatD) has already been implicated in the degradation of αSyn[154]. Accordingly, an overexpression of CatD seems to prevent αSyn-induced degeneration in several model organisms[155]. Our group has shown that Pep4 overexpression reduces cell death caused by αSyn in yeast as well[143].

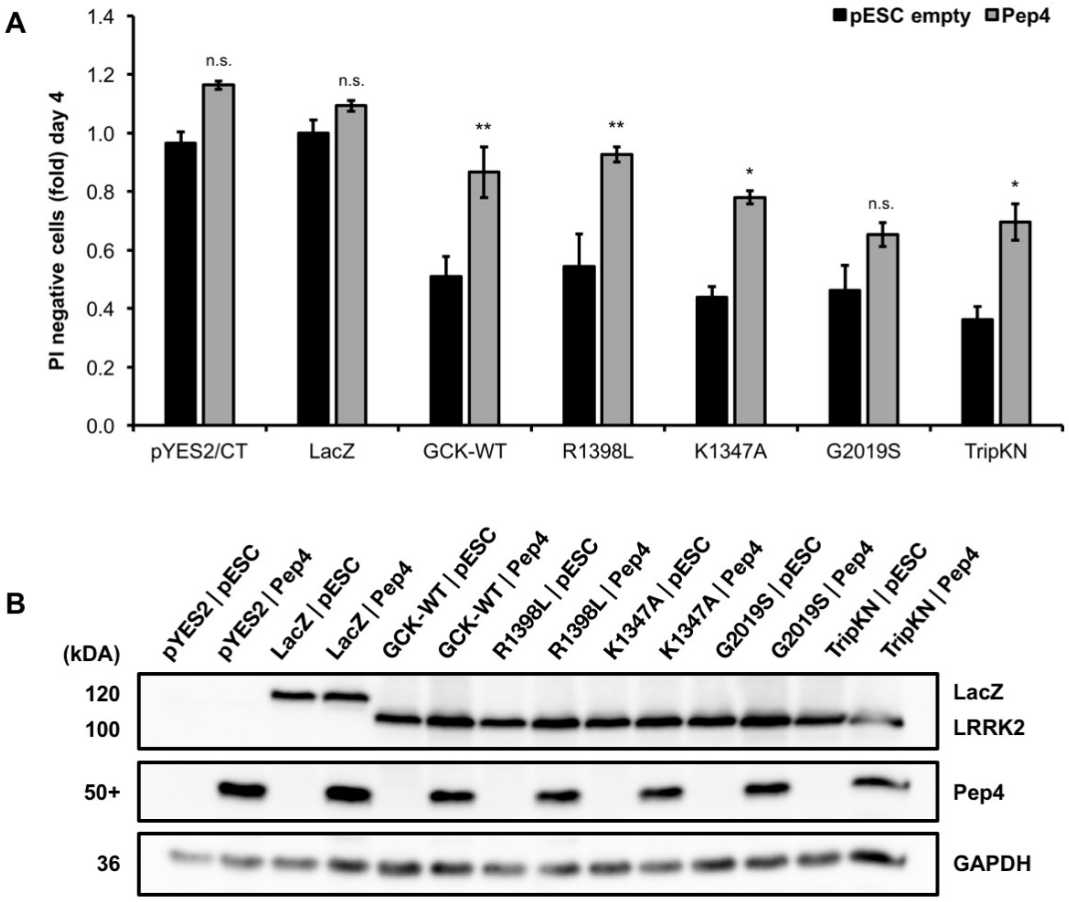

Figure 16: Pep4 overexpression reduces LRRK2 toxicity. Yeast cells heterologously expressing human LRRK2-GCK in its wild type form (GCK-WT) and several mutant alleles (R1398L, K1347A, G2019S, TripKN) compared to cells expressing LacZ or the empty vector. The viability of cells overexpressing Pep4 compared to cells harbouring empty pESC-HIS, the vector used for Pep4 expression. (**A**) Flow cytometric quantification of PI stained cells as a signifier of cell death on day 3. Mean ± S.E.M., , $n = 4$, ** = $P < 0.01$, * = $P < 0.05$, n.s. = not significant. (**B**) Immunoblot expression control. The blot was probed with antibodies directed against the V5 epitope to detect the V5-tagged LacZ and LRRK2, against FLAG epitope to detect the FLAG-tagged Pep4 and against GAPDH as a loading control.

We investigated whether overexpression of Pep4 could exert a similar cytoprotective influence on LRRK2-related death in our yeast model. High levels of Pep4 significantly reduced cell death for the LRRK2 wild type and all mutants – except for G2019S – and raised their viability to a level that was comparable to that of the control (Figure 16A). There was no significant change in viability for the controls. Notably, the viability of cells overexpressing Pep4 and expressing GCK wild type and the R1389L, K1347A and TripKN was not significantly different to the viability of the control without Pep4 overexpression. This suggests that Pep4 overexpression was able to fully rescue LRRK2 toxicity. Pep4 expression was confirmed via immunoblot (Figure 16B).

4.5 Levels of Cellular Pep4 Are Unaltered by LRRK2 Expression

Having established that Pep4 overexpression alleviates LRRK2-induced cell death in our model (see above), we considered that cellular Pep4 levels might be impaired by LRRK2. A recent study in mice has shown that there is a deficit in trafficking of the Pep4 homologue CatD to the late endosome in neurons overexpressing αSyn[156]. This leads to reduced levels of CatD in the lysosome and an impairment of αSyn degradation. Similarly, our group has shown a mislocalisation of Pep4 and its sorting receptor upon αSyn overexpression in yeast[143].

To explore whether there is a defect in Pep4 trafficking in our LRRK2 model, we analysed the cellular levels of Pep4 by immunoblotting using endogenously HA-tagged Pep4. Pep4 levels were not affected by expression of LRRK2 and its mutants throughout the ageing (Figure 17), suggesting that Pep4 trafficking is not impaired in our model.

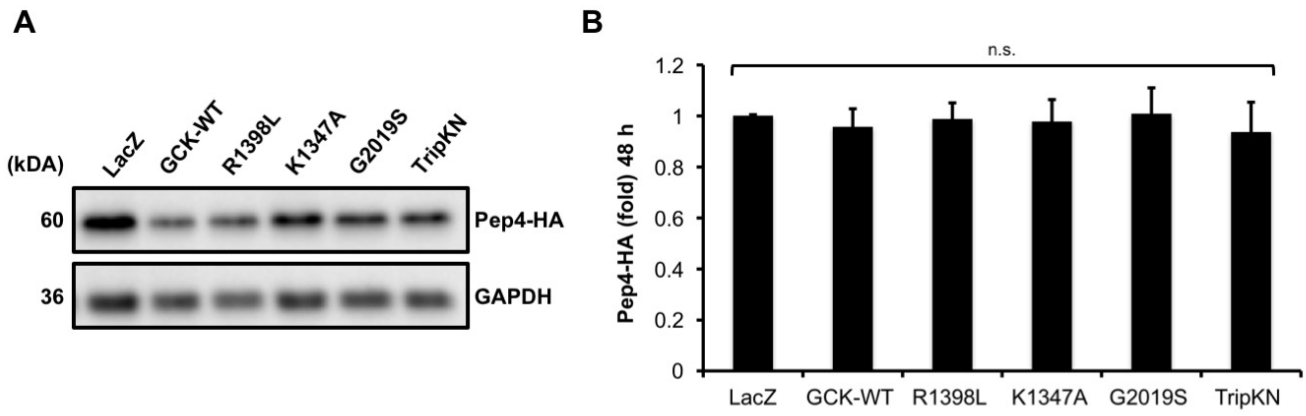

Figure 17: Vacuolar Pep4 levels are not affected by LRRK2 toxicity. Analysis of protein extracts from endogenously HA-tagged Pep4 harbouring yeast cells heterologously expressing human LRRK2-GCK in its wild type form (GCK-WT) and several mutant alleles (R1398L, K1347A, G2019S, TripKN) compared to cells expressing LacZ. (**A**) Representative immunoblot. The blot was probed with antibodies directed against the HA epitope to detect the HA-tagged Pep4 and against GAPDH as a loading control. (**B**) Quantitative comparison of the detected Pep4 levels using data obtained from immunoblots in (**A**). Mean ± S.E.M., $n = 4$, n.s. = not significant.

4.6 Co-expression of LRRK2 and αSyn^{EGFP} Shows No Co-toxicity

Evidence from several studies suggests that LRRK2 interferes with autophagic processes[99,110], but it is still unknown how this interference occurs. Similarly, αSyn has been implicated in obstructing autophagy[157]. As both of these proteins are involved in blocking the same pathway, it has been proposed that their function may be interconnected – potentially by phosphorylation of αSyn via the LRRK2 kinase – although this has yet to be shown[158]. To investigate any interaction or co-toxicity between the proteins, it would be beneficial to establish a co-expression model. Our group has already previously investigated αSyn within a well-established model of heterologous expression in yeast[159,160,153,161]. However, this model would be insufficient for the exploration of co-toxicity as αSyn would lead to excessive cell death before the onset of LRRK2 toxicity. We therefore decided to co-express the less toxic αSyn^{EGFP} [162,160] within our LRRK2 model. The expression of αSyn^{EGFP} was confirmed via immunoblotting (Figure 20A) and fluorescence microscopy (Figure 19). The micrographs showed that αSyn^{EGFP} formed aggregates as has been described previously[162]; this aggregation could be verified by immunoblotting under native conditions (Figure 20B). There was no significant difference between αSyn^{EGFP} aggregation in the presence of LRRK2 and the controls (Figure 18).

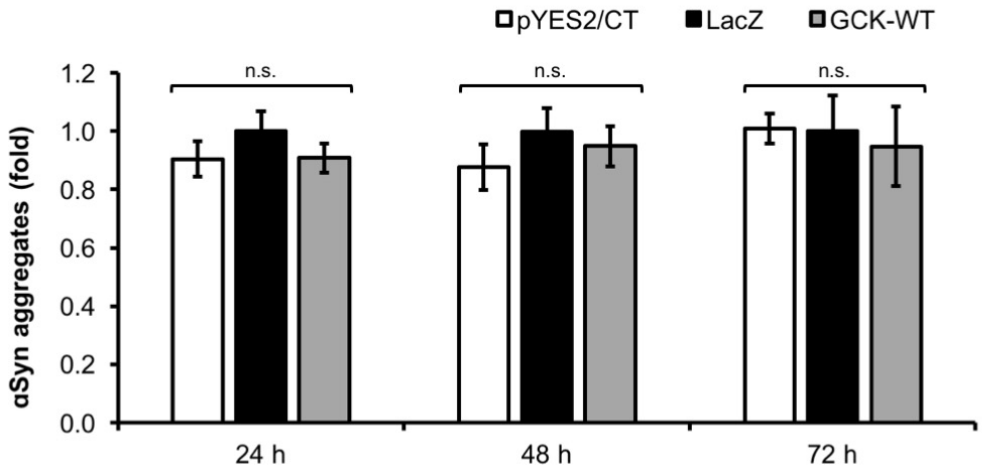

Figure 18: LRRK2 co-expression did not lead to a significant difference in αSyn^{EGFP} aggregation. Quantification of αSyn^{EGFP} aggregates in yeast cells heterologously expressing human LRRK2-GCK in its wild type form (GCK-WT), expressing the LacZ control or harbouring the empty vector using micrographs shown in (**19**). Mean ± S.E.M., n = 6-8, n.s. = not significant.

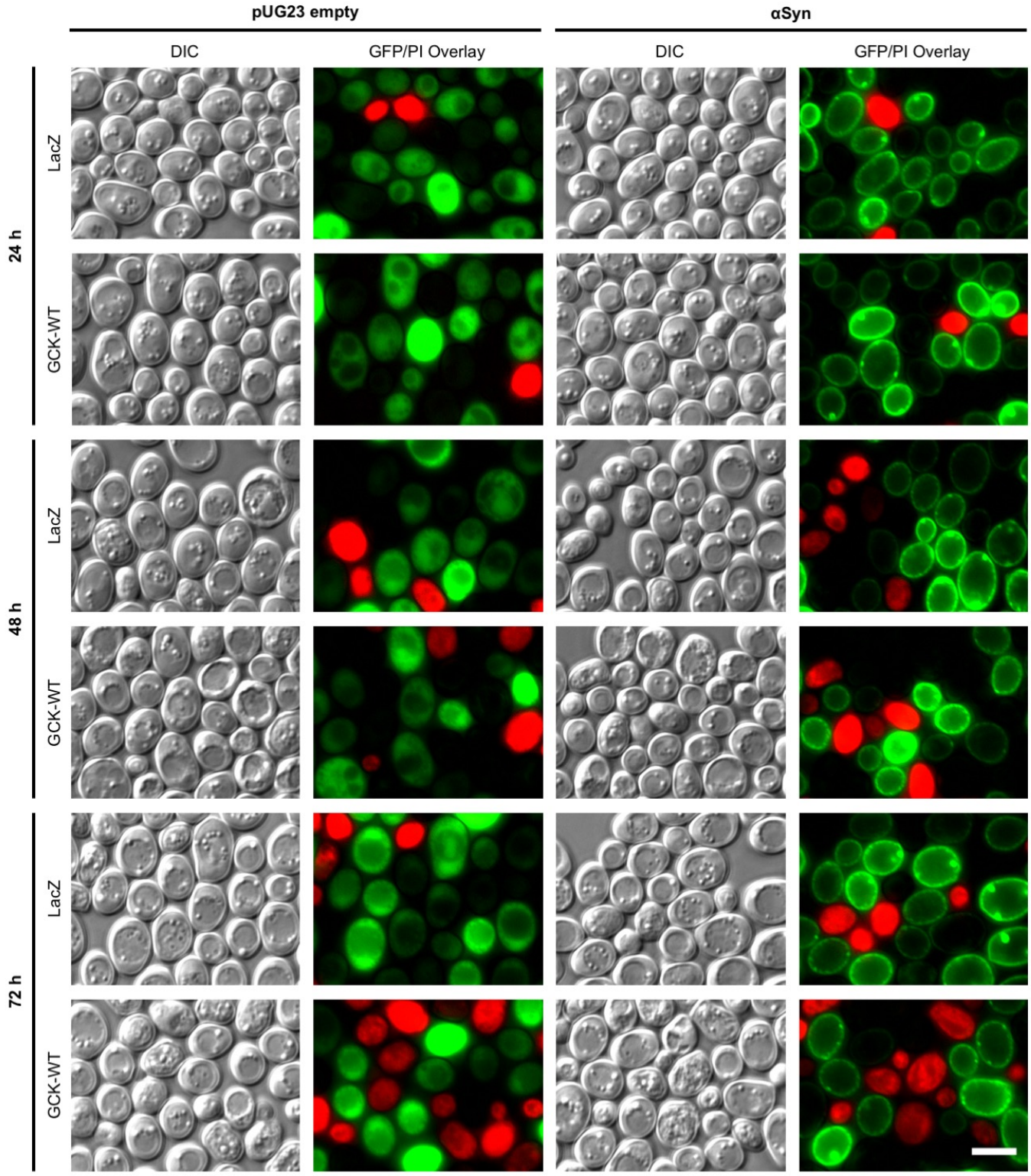

Figure 19: LRRK2 toxicity has no influence on αSyn^{EGFP} aggregation. Differential interference contrast (DIC) and fluorescent microscope analysis of PI stained yeast cells heterologously expressing human LRRK2. Cells were either expressing αSyn^{EGFP} or free GFP via the corresponding pUG23 vector control. LRRK2-GCK in its wild type form (GCK-WT) compared to cells expressing LacZ. Scale bar represents 5 μm. Representative micrographs were taken at 24, 40, 48 and 72 hours after induction of LRRK2-GCK expression.

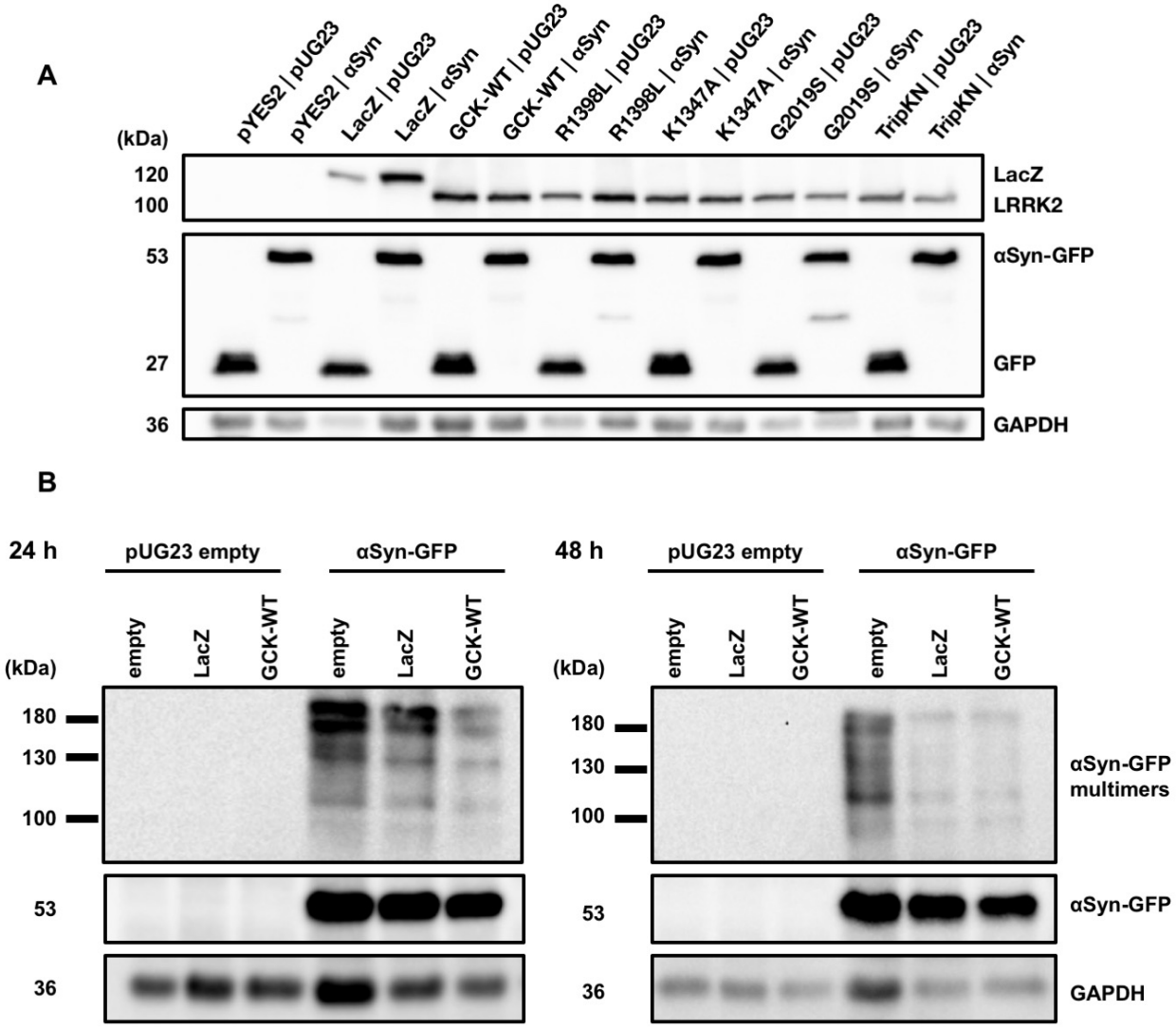

Figure 20: αSyn^{EGFP} was expressed and formed aggregates. Immunoblot analysis of protein extracts from cells co-expressing αSyn^{EGFP} and LRRK2-GCK in its wild type form (GCK-WT) and several mutant alleles (R1398L, K1347A, G2019S, TripKN) or the LacZ control, or harbouring the corresponding empty vector controls (pUG23 for αSyn^{EGFP}, pYES2/CT for LRRK2 and LacZ). (**A**) Expression control. Blot was probed with antibodies directed against the V5 epitope to detect LRRK2 and LacZ, GFP to detect αSyn^{EGFP} and GAPDH as a loading control. (**B**) αSyn^{EGFP} aggregates blotted under native conditions. Blots were probed with antibodies directed against the FLAG epitope to detect αSyn^{EGFP} and GAPDH as a loading control.

As for cell death, co-expression of αSyn^{EGFP} appears to have no significant effect on LRRK2 toxicity. The only significant impact was observed for the R1398L mutant on day 3, when LRRK2 toxicity typically becomes apparent; however, this difference was absent at day 4 (Figure 21).

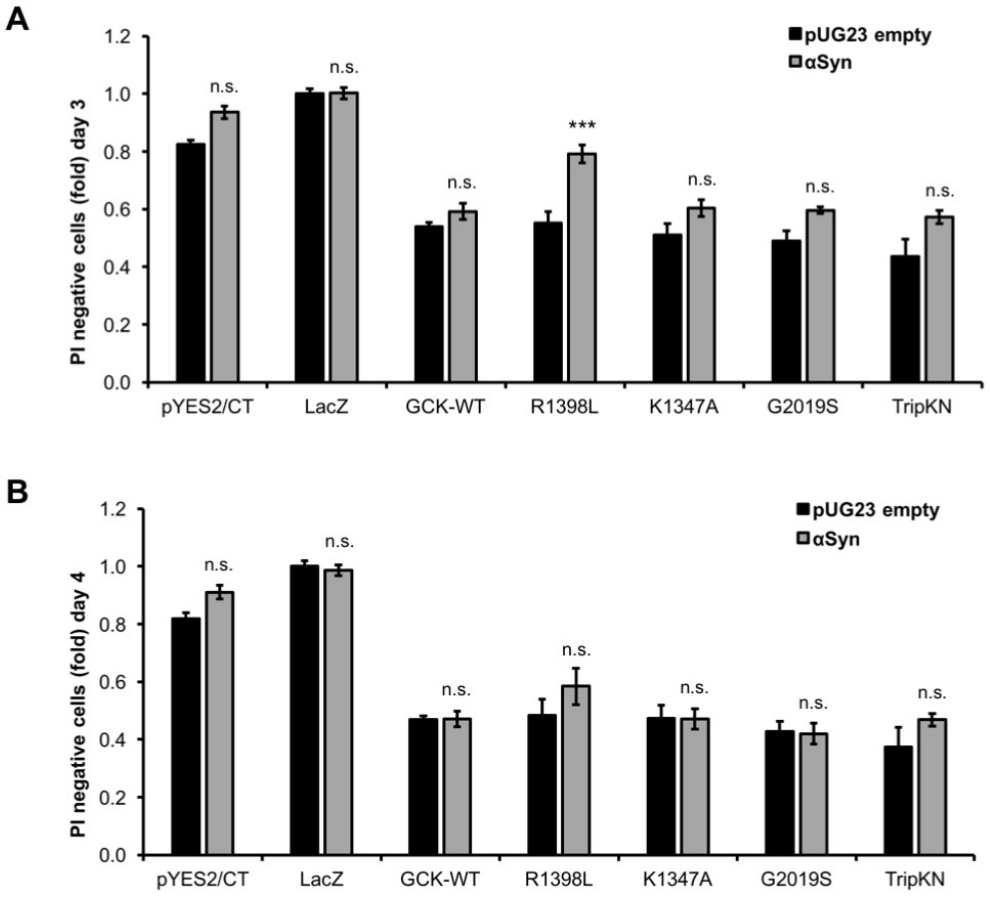

Figure 21: Co-expression of αSyn^{EGFP} has no significant effect on LRRK2 toxicity. Yeast cells co-expressing αSyn^{EGFP} and LRRK2-GCK in its wild type form (GCK-WT) and several mutant alleles (R1398L, K1347A, G2019S, TripKN) or the LacZ control, or harbouring the corresponding empty vector controls (pUG23 for αSyn^{EGFP}, pYES2/CT for LRRK2 and LacZ) were analysed. Flow cytometric quantification of PI stained cells as a signifier of cell death on day 3 (**A**) and day 4 (**B**). Mean ± S.E.M., , n = 3-4, *** = $P < 0.001$, n.s. = not significant compared to the corresponding pUG23 empty control value.

5. Discussion

LRRK2 mutants are an important factor in the pathology of familial PD. In spite of this, their molecular workings remain uncertain. The aim of this study was to investigate the mechanism by which LRRK2 and its mutated forms affect autophagy in yeast and look at a possible interaction between LRRK2 and αSyn. We confirmed an impairment of autophagy by LRRK2 shown in other model systems in our aging yeast model and showed that pharmacological autophagy induction via rapamycin reduces LRRK2 toxicity. The autophagy block was not caused by changes in vacuolar acidification. Overexpression of the vacuolar protease Pep4 proved protective against LRRK2-induced cell death, while cellular protein levels of Pep4 were shown to be unaffected by LRRK2. We successfully co-expressed αSyn, but observed no co-toxicity with LRRK2 in our model.

5.1 How Does LRRK2 Affect Autophagy?

Molecular and physiological changes leading up to PD likely happen long before symptoms are recognisable. Research into the details of these mechanisms and the discovery of drug targets is therefore crucial to disease prevention.

While the link between LRRK2 and autophagy is widely recognised, studies of this connection have led to contradictory results (see above). Notably, the G2019S mutant decreased autophagy in iPSC-derived human dopaminergic neurons[98] – which analyse human physiology and are therefore arguably the closest model next to actual patients. We confirmed an impairment of autophagy by LRRK2 in our model via GFP-Atg8 assay. The *LRRK2* mutations had no apparent effect on the autophagy block, suggesting that it is caused by neither enzymatic activity, or only needs one of the two enzymatic domains to be functional. For the G2019S mutation this is conform with a study in mammalian cells, where the LRRK2 wild type and mutation led to the same degree of autophagosome accumulation[92].

Although GFP-tagged Atg8 is a well established tool for monitoring autophagy, it is not sufficient to completely confirm an autophagy block. For one, it measures flux of an autophagic carrier which does not necessarily equal cargo flux[149]. Another issue is that while autophagosomes can be observed and counted on micrographs, there is no guarantee that this quantification is accurate; it is possible that not all autophagosomes are visible or artefacts may be counted. The GFP-tag itself may also influence the system, so it is important to verify results with methods that do not require this tag. Further techniques that might be employed are

enzymatic assays such as the Pho8Δ60 assay, which allows for easier quantification and the use of electron microscopy to observe autophagosome accumulation.

Next, we set out to investigate what factors are impairing autophagy in this context. Cytosolic and vacuolar pH homeostasis are crucial to many cellular processes including autophagy. Impaired vacuolar acidification allows for the initial steps of autophagy to proceed but inhibits fusion of the autophagosome with the vacuole, leading to an accumulation of autophagosomes[127] – similar to the phenotype we have observed under LRRK2 toxicity. In addition, our group has previously shown that αSyn causes problems with pH homeostasis in yeast[143]. However, we observed no pH changes in relation to LRRK2. This makes it less likely that LRRK2 leads to a shift in acidification, but has to be confirmed by additional methods to account for limitations inherent to our technique. The rising cellular acidification in ageing yeast renders evaluation with quinacrine staining under the fluorescent microscope impossible at later time points due to strong background fluorescence. While αSyn-related acidification occurs early enough to avoid this difficulty[143], the same is not guaranteed for LRRK2, which has toxic effects at a much later point in the ageing. Confirmation using a different pH indicator might offer more conclusive information. Additionally, verification in higher organisms is required, as there are differences in pH regulation compared to yeast[135].

Another key player in autophagy are vacuolar proteases which degrade the cargo. Pep4 is not only an important vacuolar protease but its lysosomal mammalian orthologue CatD has also been implicated in the degradation of αSyn[154]. Accordingly, an overexpression of CatD seems to act neuroprotectively against αSyn-induced degeneration in several model organisms[155]. Our group has shown that Pep4 overexpression reduces cell death caused by αSyn in yeast as well[143]. The same proved true for LRRK2 toxicity. Pep4 overexpression improved cell viability to such an extent that it was lifted to a level on par with the control. Notably, cell death of the G2019S mutant was not improved. This could indicate that increased LRRK2 kinase activity counteracts the beneficial effects of increased Pep4 protein levels. However, the data are preliminary and further repeat experiments may show this to be an artefact. Additionally, it should be remarked that protection against αSyn toxicity via Pep4 overexpression has been shown to work independently of autophagy[143] and general lifespan extension of yeast cells by Pep4 overexpression is not mediated by autophagy[163]. It is unclear whether the same is true for LRRK2.

A recent study in mice has shown that there is a deficit in trafficking of CatD to the late endosome in neurons overexpressing αSyn[156]. This leads to reduced protein levels of CatD in the lysosome and an impairment of αSyn degradation. Similarly, our group has shown a

mislocalisation of Pep4 and its sorting receptor upon αSyn overexpression in yeast[143]. Notably, CatD levels are reduced in post-mortem brain samples of PD patients as well[156] and it has been proposed that the detection of lysosomal proteins could function as a marker for lysosomal dysfunction in PD and perhaps as a biomarker for PD itself[164]. However, in our LRRK2 model, Pep4 levels were not decreased, suggesting that Pep4 trafficking was not impaired. This does not mean that Pep4 is not involved in LRRK2 toxicity – Pep4 activity could be affected as well and should be addressed in future experiments. This is of particular interest as a decrease in CatD activity in response to αSyn expression has been reported[156].

5.2 Induction of Autophagy: Rapamycin As a Possible Treatment For Parkinson's Disease?

We introduced three drugs into our model system to stimulate autophagy in an attempt to alleviate LRRK2 toxicity: Calcium, spermidine and rapamycin. Calcium and spermidine were unable to rescue LRRK2 toxicity. Although the fact that calcium signalling has an impact on autophagy is well established, the details of this connection are uncertain[152]; some studies report autophagy activation[165,166,167] while others describe inhibition[168]. It is possible that calcium stimulates (or inhibits) autophagy in ways that do not counteract the influence of LRRK2. That spermidine led to cell death in our model is likely to be an artefact, as it is widely accepted that spermidine has a positive effect on yeast viability[151,169].

On the other hand, rapamycin did prove protective against LRRK2 toxicity. It increased viability and survival, without affecting LRRK2 expression levels. Quantification of cell count and size showed that rapamycin did not affect cell proliferation, only cell death. This observation is especially of interest as rapamycin is already clinically approved for human treatment. It finds use in a diverse set of areas, including as an immunosuppressant to prevent the rejection of organ transplants, in cancer treatment to inhibit tumour proliferation and in cardiovascular disease[170]. Autophagy modulation has been suggested as a treatment for several neurodegenerative diseases. Rapamycin itself has been shown to act neuroprotectively in several models of neurodegenerative diseases including Alzheimer's disease, Huntington's disease and spinocerebellar ataxia type 3[171]. Furthermore, it decreases dopaminergic cell death in cell culture and mouse models of PD[172,173]. Induction of autophagy by various substances has been shown to reduce αSyn toxicity in several model of PD as well[174,175,176], marking it an increasingly promising approach for therapeutic intervention.

Nonetheless, the the precise nature of autophagic defects needs to be defined in order to properly target treatment. If there is no dysfunction in the formation of autophagosomes, but rather a block in autophagic flux such as we have observed, further activation of autophagy could lead to detrimental effects. However, in this regard it is notable that in post-mortem brain samples from PD patients, where autophagosomes were shown to accumulate in a similar manner[173,177], rapamycin restored the impaired lysosome-mediated clearance of autophagosomes[173]. This is likely because rapamycin also leads to increased lysosomal biogenesis and thus provides more functional lysosomes that can potentially fuse with autophagosomes, as was shown in a PD mouse model[173]. Lastly, even if rapamycin proves to be an effective treatment or preventive tool for PD several hurdles have to be overcome. For example, it has to be defined at what stage of the disease it should be administered and what side effects might arise from long-term administration.

5.3 LRRK2 and α-Synuclein: Colluding Players in the Pathology of Parkinson's Disease?

Not only LRKK2, but also αSyn has been implicated in impairment of autophagy[157]. As both proteins are involved in obstructing the same pathway, it has been proposed that their function may be interconnected[158]. Furthermore, both proteins have been linked to microtubule dynamics and axonal transport[158]. It has been proposed that the LRRK2 kinase may phosphorylate αSyn, but this has yet to be conclusively shown and it has also been suggested that LRRK2 may instead work upstream of αSyn[158]. Thus, there is a need for clarification through further models that study the interplay between LRRK2 and αSyn. Yeast offers the possibility to study this interaction without influence from other mammalian proteins that the players may interact with physiologically. This makes it an attractive model for investigation, although it necessitates future replication in higher organisms to confirm the relevance of the results.

We successfully co-expressed αSyn^{EGFP} and LRRK2 and observed αSyn aggregates as previously described[162,160]; although it is unclear whether the detected aggregates solely consisted of αSyn oligomers or also contained additional proteins interacting with αSyn. However, LRRK2 appeared to have neither positive nor negative effect on αSyn aggregation. It is possible that this occurs because the EGFP-tag obstructs the interaction between the proteins or other αSyn interactions within the cell. We chose EGFP-tagged αSyn because its lessened toxicity makes it possible to study colonies on day 3, when LRRK2 toxicity is first observed, but this decrease in

toxicity also suggests that αSyn^{EGFP} operates differently than αSyn. We therefore can make no conclusive statement about a potential link between LRRK2 and αSyn. A different model needs to be developed to study this interaction.

6. Abbreviations

APS	ammoniumperoxo-disulphate
BSA	bovine serum albumin
C. elegans	*Caenorhabditis elegans*
CAPS	N-cyclohexyl-3-aminopropanesulfonic acid
CatD	cathepsin D
ddH2O	double destilled water
DHE	dihydroethidium
DIC	differential interference contrast
DMSO	dimethyl sulfoxide
E. coli	*Escherichia coli*
EDTA	ethylenediaminetetraacetic acid
EGFP	enhanced green fluorescent protein
FACS	fluorescence activated cell sorting
GAPDH	glyceraldehyd-3-phosphate dehydrogenase
GFP	green fluorescent protein
HCl	hydrochloric acid
HEPES	4-(2-hydroxyethyl)-1-piperazineethanesulfonic acid
iPSC	induced pluripotent stem cells
K_2HPO_4	dipotassium hydrogenphosphate
KH_2PO_4	potassium dihydrogen phosphate
LacZ	β-galactosidase
LB	lysogeny broth
LRRK2	Leucine-rich repeat kinase 2
mL	millilitre
mM	millimolar

NaCl	natriumchlorid
NaOH	sodium hydroxide
nM	nanomolar
OD	optical density
ONC	over night culture
PAS	phagophore assembly site
PD	Parkinson's disease
PE	phosphatidylethanolamine
PI	propidium iodide
rpm	revolutions per minute
S. cerevisiae	*Saccharomyces cerevisiae*
S.E.M.	standard error of the mea
SDS	sodium dodecyl sulfate
SMD	synthetic minimal dextrose
SMG	synthetic minimal galactose
SNc	substantia nigra pars compacta
TEMED	N,N,N',N'-tetramethylethylendiamin
TOR	target of rapamycin
TORC1	TOR complex 1
TORC2	TOR complex 2
Tris	tris(hydroxymethyl)aminomethane
YNB	yeast nitrogen base
YPD	yeast peptone dextrose
αSyn	α-synuclein
μL	microlitre
μm	micrometre

7. References

1. Hirsch, L., Jette, N., Frolkis, A., Steeves, T. & Pringsheim, T. The Incidence of Parkinson's Disease: A Systematic Review and Meta-Analysis. *Neuroepidemiology* **46,** 292–300 (2016).

2. Pringsheim, T., Jette, N., Frolkis, A. & Steeves, T. D. L. The prevalence of Parkinson's disease: A systematic review and meta-analysis. *Mov. Disord.* **29,** 1583–1590 (2014).

3. Alzheimer's Association. 2016 Alzheimer's disease facts and figures. *Alzheimers. Dement.* **12,** 459–509 (2016).

4. Kowal, S. L., Dall, T. M., Chakrabarti, R., Storm, M. V. & Jain, A. The current and projected economic burden of Parkinson's disease in the United States. *Mov. Disord.* **28,** 311–318 (2013).

5. Gustavsson, A. *et al.* Cost of disorders of the brain in Europe 2010. *Eur. Neuropsychopharmacol.* **21,** 718–779 (2011).

6. Sveinbjornsdottir, S. The clinical symptoms of Parkinson's disease. *J. Neurochem.* **139,** 318–324 (2016).

7. Khoo, T. K. *et al.* The spectrum of nonmotor symptoms in early Parkinson disease. *Neurology* **80,** 276–281 (2013).

8. Yuan, H. *et al.* Treatment strategies for Parkinson's disease. *Neurosci. Bull.* **26,** 66–76 (2010).

9. Kandel, E. R., Schwartz, J. H., Jessell, T. M., Siegelbaum, S. A. & Hudspeth, A. J. *Principles of Neural Science*. (The McGraw-Hill Companies, Inc., 2013).

10. Dickson, D. W. *et al.* Neuropathological assessment of Parkinson's disease: refining the diagnostic criteria. *Lancet Neurol.* **8,** 1150–1157 (2009).

11. Dauer, W. & Przedborski, S. Parkinson's disease: mechanisms and models. *Neuron* **39,** 889–909 (2003).

12. Dickson, D. W. Parkinson's Disease and Parkinsonism: Neuropathology. *Cold Spring Harb. Perspect. Med.* **2,** a009258–a009258 (2012).

13. Braak, H. & Del Tredici, K. in *Neuroanatomy and Pathology of Sporadic Parkinson's Disease* 18–20 (Springer Berlin Heidelberg, 2009).

14. Goedert, M., Spillantini, M. G., Del Tredici, K. & Braak, H. 100 years of Lewy pathology. *Nat. Rev. Neurol.* **9,** 13–24 (2012).

15. Braak, H. & Del Tredici, K. in *Neuroanatomy and Pathology of Sporadic Parkinson's Disease* 1–8 (Springer Berlin Heidelberg, 2009).

16. Spillantini, M. G., Crowther, R. A., Jakes, R., Hasegawa, M. & Goedert, M. alpha-Synuclein in filamentous inclusions of Lewy bodies from Parkinson's disease and dementia with lewy bodies. *Proc. Natl. Acad. Sci. U. S. A.* **95,** 6469–73 (1998).

17. Tu, P. *et al.* Glial cytoplasmic inclusions in white matter oligodendrocytes of multiple system atrophy brains contain insoluble alpha-synuclein. *Ann. Neurol.* **44,** 415–422 (1998).

18. Spillantini, M. G. *et al.* α-Synuclein in Lewy bodies. *Nature* **388,** 839–840 (1997).

19. Surguchov, A. in *International review of cell and molecular biology* **270,** 225–317 (2008).

20. Iwai, A. *et al.* The precursor protein of non-A beta component of Alzheimer's disease amyloid is a presynaptic protein of the central nervous system. *Neuron* **14,** 467–75 (1995).

21. Benskey, M. J., Perez, R. G. & Manfredsson, F. P. The contribution of alpha synuclein to neuronal survival and function - Implications for Parkinson's disease. *J. Neurochem.* **137,** 331–359 (2016).

22. Burré, J. *et al.* Alpha-synuclein promotes SNARE-complex assembly in vivo and in vitro. *Science* **329,** 1663–7 (2010).

23. Braak, H. & Del Tredici, K. in *Neuroanatomy and Pathology of Sporadic Parkinson's Disease* 9 (Springer Berlin Heidelberg, 2009).

24. Doherty, K. M. *et al.* Parkin disease: a clinicopathologic entity? *JAMA Neurol.* **70,** 571–9 (2013).

25. Poulopoulos, M., Levy, O. A. & Alcalay, R. N. The neuropathology of genetic Parkinson's disease. *Mov. Disord.* **27,** 831–842 (2012).

26. Parkkinen, L. *et al.* Disentangling the relationship between lewy bodies and nigral neuronal loss in Parkinson's disease. *J. Parkinsons. Dis.* **1,** 277–86 (2011).

27. Noyce, A. J. *et al.* Meta-analysis of early nonmotor features and risk factors for Parkinson disease. *Ann. Neurol.* **72,** 893–901 (2012).

28. Priyadarshi, A., Khuder, S. A., Schaub, E. A. & Shrivastava, S. A meta-analysis of Parkinson's disease and exposure to pesticides. *Neurotoxicology* **21,** 435–40 (2000).

29. Klein, C. & Westenberger, A. Genetics of Parkinson's disease. *Cold Spring Harb. Perspect. Med.* **2,** a008888 (2012).

30. Trinh, J. & Farrer, M. Advances in the genetics of Parkinson disease. *Nat. Rev. Neurol.* **9,** 445–454 (2013).

31. Polymeropoulos, M. H. *et al.* Mutation in the alpha-synuclein gene identified in families with Parkinson's disease. *Science* **276,** 2045–7 (1997).

32. Corti, O., Lesage, S. & Brice, A. What Genetics Tells us About the Causes and Mechanisms of Parkinson's Disease. *Physiol. Rev.* **91,** 1161–1218 (2011).

33. Vilariño-Güell, C. *et al.* VPS35 Mutations in Parkinson Disease. *Am. J. Hum. Genet.* **89,** 162–167 (2011).

34. Chartier-Harlin, M.-C. *et al.* Translation initiator EIF4G1 mutations in familial Parkinson disease. *Am. J. Hum. Genet.* **89,** 398–406 (2011).

35. Vilariño-Güell, C. *et al.* DNAJC13 mutations in Parkinson disease. *Hum. Mol. Genet.* **23,** 1794–801 (2014).

36. Funayama, M. *et al.* CHCHD2 mutations in autosomal dominant late-onset Parkinson's disease: a genome-wide linkage and sequencing study. *Lancet. Neurol.* **14,** 274–82 (2015).

37. Aras, S. *et al.* MNRR1 (formerly CHCHD2) is a bi-organellar regulator of

mitochondrial metabolism. *Mitochondrion* **20,** 43–51 (2015).

38. Periquet, M. *et al.* Parkin mutations are frequent in patients with isolated early-onset parkinsonism. *Brain* **126,** 1271–1278 (2003).

39. Narendra, D., Walker, J. E. & Youle, R. Mitochondrial quality control mediated by PINK1 and Parkin: links to parkinsonism. *Cold Spring Harb. Perspect. Biol.* **4,** a011338 (2012).

40. Bonifati, V. *et al.* Mutations in the DJ-1 gene associated with autosomal recessive early-onset parkinsonism. *Science* **299,** 256–9 (2003).

41. Mata, I. F., Wedemeyer, W. J., Farrer, M. J., Taylor, J. P. & Gallo, K. A. LRRK2 in Parkinson's disease: protein domains and functional insights. *Trends Neurosci.* **29,** 286–93 (2006).

42. Greggio, E. *et al.* The Parkinson Disease-associated Leucine-rich Repeat Kinase 2 (LRRK2) Is a Dimer That Undergoes Intramolecular Autophosphorylation. *J. Biol. Chem.* **283,** 16906–16914 (2008).

43. Mandemakers, W., Snellinx, A., O'Neill, M. J. & de Strooper, B. LRRK2 expression is enriched in the striosomal compartment of mouse striatum. *Neurobiol. Dis.* **48,** 582–593 (2012).

44. Westerlund, M. *et al.* Developmental regulation of leucine-rich repeat kinase 1 and 2 expression in the brain and other rodent and human organs: Implications for Parkinson's disease. *Neuroscience* **152,** 429–436 (2008).

45. Hakimi, M. *et al.* Parkinson's disease-linked LRRK2 is expressed in circulating and tissue immune cells and upregulated following recognition of microbial structures. *J. Neural Transm.* **118,** 795–808 (2011).

46. Biskup, S. *et al.* Localization of LRRK2 to membranous and vesicular structures in mammalian brain. *Ann. Neurol.* **60,** 557–569 (2006).

47. Alegre-Abarrategui, J. *et al.* LRRK2 regulates autophagic activity and localizes to specific membrane microdomains in a novel human genomic reporter cellular model. *Hum. Mol. Genet.* **18,** 4022–4034 (2009).

48. Wakabayashi, K., Tanji, K., Mori, F. & Takahashi, H. The Lewy body in

Parkinson's disease: Molecules implicated in the formation and degradation of α-synuclein aggregates. *Neuropathology* **27,** 494–506 (2007).

49. Di Fonzo, A. *et al.* Comprehensive analysis of the LRRK2 gene in sixty families with Parkinson's disease. *Eur. J. Hum. Genet.* **14,** 322–331 (2006).

50. Nichols, W. C. *et al.* LRRK2 mutation analysis in Parkinson disease families with evidence of linkage to PARK8. *Neurology* **69,** 1737–1744 (2007).

51. Johnson, J. *et al.* Comprehensive Screening of a North American Parkinson's Disease Cohort for LRRK2 Mutation. *Neurodegener. Dis.* **4,** 386–391 (2007).

52. Lesage, S. *et al.* Molecular analyses of the LRRK2 gene in European and North African autosomal dominant Parkinson's disease. *J. Med. Genet.* **46,** 458–464 (2009).

53. Paisán-Ruíz, C., Nath, P., Washecka, N., Gibbs, J. R. & Singleton, A. B. Comprehensive analysis of LRRK2 in publicly available Parkinson's disease cases and neurologically normal controls. *Hum. Mutat.* **29,** 485–490 (2008).

54. Nuytemans, K., Theuns, J., Cruts, M. & Van Broeckhoven, C. Genetic etiology of Parkinson disease associated with mutations in the SNCA, PARK2, PINK1, PARK7, and LRRK2 genes: a mutation update. *Hum. Mutat.* **31,** 763–780 (2010).

55. Corti, O., Lesage, S. & Brice, A. What genetics tells us about the causes and mechanisms of Parkinson's disease. *Physiol. Rev.* **91,** 1161–218 (2011).

56. West, A. B. *et al.* Parkinson's disease-associated mutations in leucine-rich repeat kinase 2 augment kinase activity. *Proc. Natl. Acad. Sci. U. S. A.* **102,** 16842–7 (2005).

57. Greggio, E. & Cookson, M. R. Leucine-rich repeat kinase 2 mutations and Parkinson's disease: three questions. *ASN Neuro* **1,** (2009).

58. Giasson, B. I. *et al.* Biochemical and pathological characterization of Lrrk2. *Ann. Neurol.* **59,** 315–22 (2006).

59. Taylor, J. P., Mata, I. F. & Farrer, M. J. LRRK2: a common pathway for parkinsonism, pathogenesis and prevention? *Trends Mol. Med.* **12,** 76–82

(2006).

60. Gloeckner, C. J. *et al.* The Parkinson disease causing LRRK2 mutation I2020T is associated with increased kinase activity. *Hum. Mol. Genet.* **15,** 223–232 (2006).

61. Jaleel, M. *et al.* LRRK2 phosphorylates moesin at threonine-558: characterization of how Parkinson's disease mutants affect kinase activity. *Biochem. J.* **405,** 307–317 (2007).

62. Liao, J. *et al.* Parkinson disease-associated mutation R1441H in LRRK2 prolongs the "active state" of its GTPase domain. *Proc. Natl. Acad. Sci.* **111,** 4055–4060 (2014).

63. Lewis, P. A. *et al.* The R1441C mutation of LRRK2 disrupts GTP hydrolysis. *Biochem. Biophys. Res. Commun.* **357,** 668–71 (2007).

64. Daniëls, V. *et al.* Insight into the mode of action of the LRRK2 Y1699C pathogenic mutant. *J. Neurochem.* **116,** 304–15 (2011).

65. Fu, X. *et al.* LRRK2 G2385R and LRRK2 R1628P increase risk of Parkinson's disease in a Han Chinese population from Southern Mainland China. *Parkinsonism Relat. Disord.* **19,** 397–398 (2013).

66. Ross, O. A. *et al.* Analysis of Lrrk2 R1628P as a risk factor for Parkinson's disease. *Ann. Neurol.* **64,** 88–92 (2008).

67. Funayama, M. *et al.* Leucine-Rich Repeat kinase 2 G2385R variant is a risk factor for Parkinson disease in Asian population. *Neuroreport* **18,** 273–275 (2007).

68. Aasly, J. O. *et al.* Novel pathogenic LRRK2 p.Asn1437His substitution in familial Parkinson's disease. *Mov. Disord.* **25,** 2156–2163 (2010).

69. Rudenko, I. N. *et al.* The G2385R variant of leucine-rich repeat kinase 2 associated with Parkinson's disease is a partial loss-of-function mutation. *Biochem. J.* **446,** 99–111 (2012).

70. Shu, Y. *et al.* Parkinson-Related LRRK2 Mutation R1628P Enables Cdk5 Phosphorylation of LRRK2 and Upregulates Its Kinase Activity. *PLoS One* **11,**

e0149739 (2016).

71. Lee, B. D. *et al.* Inhibitors of leucine-rich repeat kinase-2 protect against models of Parkinson's disease. *Nat. Med.* **16,** 998–1000 (2010).

72. Chan, S. L., Chua, L.-L., Angeles, D. C. & Tan, E.-K. MAP1B rescues LRRK2 mutant-mediated cytotoxicity. *Mol. Brain* **7,** 29 (2014).

73. Daniel, G. & Moore, D. J. Modeling LRRK2 pathobiology in Parkinson's disease: From yeast to rodents. *Curr. Top. Behav. Neurosci.* **22,** 331–368 (2014).

74. Greggio, E. *et al.* Kinase activity is required for the toxic effects of mutant LRRK2/dardarin. *Neurobiol. Dis.* **23,** 329–341 (2006).

75. Smith, W. W. *et al.* Kinase activity of mutant LRRK2 mediates neuronal toxicity. *Nat. Neurosci.* **9,** 1231–1233 (2006).

76. Sen, S., Webber, P. J. & West, A. B. Dependence of Leucine-rich Repeat Kinase 2 (LRRK2) Kinase Activity on Dimerization. *J. Biol. Chem.* **284,** 36346–36356 (2009).

77. Berger, Z., Smith, K. A. & Lavoie, M. J. Membrane localization of LRRK2 is associated with increased formation of the highly active LRRK2 dimer and changes in its phosphorylation. *Biochemistry* **49,** 5511–23 (2010).

78. Wallings, R., Manzoni, C. & Bandopadhyay, R. Cellular processes associated with LRRK2 function and dysfunction. *FEBS J.* **282,** 2806–26 (2015).

79. Kamikawaji, S., Ito, G. & Iwatsubo, T. Identification of the Autophosphorylation Sites of LRRK2. *Biochemistry* **48,** 10963–10975 (2009).

80. Kamikawaji, S., Ito, G., Sano, T. & Iwatsubo, T. Differential Effects of Familial Parkinson Mutations in LRRK2 Revealed by a Systematic Analysis of Autophosphorylation. *Biochemistry* **52,** 6052–6062 (2013).

81. Gloeckner, C. J. *et al.* Phosphopeptide Analysis Reveals Two Discrete Clusters of Phosphorylation in the N-Terminus and the Roc Domain of the Parkinson-Disease Associated Protein Kinase LRRK2. *J. Proteome Res.* **9,** 1738–1745 (2010).

82. Taymans, J.-M. & Cookson, M. R. Mechanisms in dominant parkinsonism: The toxic triangle of LRRK2, α-synuclein, and tau. *BioEssays* **32,** 227–235 (2010).

83. Gotthardt, K., Weyand, M., Kortholt, A., Van Haastert, P. J. M. & Wittinghofer, A. Structure of the Roc–COR domain tandem of C. tepidum, a prokaryotic homologue of the human LRRK2 Parkinson kinase. *EMBO J.* **27,** 2352–2352 (2008).

84. Webber, P. J. *et al.* Autophosphorylation in the Leucine-Rich Repeat Kinase 2 (LRRK2) GTPase Domain Modifies Kinase and GTP-Binding Activities. *J. Mol. Biol.* **412,** 94–110 (2011).

85. Taymans, J.-M. *et al.* LRRK2 Kinase Activity Is Dependent on LRRK2 GTP Binding Capacity but Independent of LRRK2 GTP Binding. *PLoS One* **6,** e23207 (2011).

86. Ito, G. *et al.* GTP Binding Is Essential to the Protein Kinase Activity of LRRK2, a Causative Gene Product for Familial Parkinson's Disease. *Biochemistry* **46,** 1380–1388 (2007).

87. Liu, M. *et al.* Kinetic, Mechanistic, and Structural Modeling Studies of Truncated Wild-Type Leucine-Rich Repeat Kinase 2 and the G2019S Mutant. *Biochemistry* **50,** 9399–9408 (2011).

88. Chan, S. L. & Tan, E.-K. Targeting LRRK2 in Parkinson's disease: an update on recent developments. *Expert Opin. Ther. Targets* **21,** 601–610 (2017).

89. Ramonet, D. *et al.* Dopaminergic Neuronal Loss, Reduced Neurite Complexity and Autophagic Abnormalities in Transgenic Mice Expressing G2019S Mutant LRRK2. *PLoS One* **6,** e18568 (2011).

90. Ferree, A. *et al.* Regulation of Physiologic Actions of LRRK2: Focus on Autophagy. *Neurodegener. Dis.* **10,** 238–241 (2012).

91. Plowey, E. D., Cherra, S. J., Liu, Y.-J. & Chu, C. T. Role of autophagy in G2019S-LRRK2-associated neurite shortening in differentiated SH-SY5Y cells. *J. Neurochem.* **105,** 1048–1056 (2008).

92. Gómez-Suaga, P. *et al.* Leucine-rich repeat kinase 2 regulates autophagy

through a calcium-dependent pathway involving NAADP. *Hum. Mol. Genet.* **21,** 511–525 (2012).

93. Bravo-San Pedro, J. M. *et al.* The LRRK2 G2019S mutant exacerbates basal autophagy through activation of the MEK/ERK pathway. *Cell. Mol. Life Sci.* **70,** 121–136 (2013).

94. Manzoni, C. *et al.* Pathogenic Parkinson's disease mutations across the functional domains of LRRK2 alter the autophagic/lysosomal response to starvation. *Biochem. Biophys. Res. Commun.* **441,** 862–866 (2013).

95. Manzoni, C. *et al.* Inhibition of LRRK2 kinase activity stimulates macroautophagy. *Biochim. Biophys. Acta - Mol. Cell Res.* **1833,** 2900–2910 (2013).

96. Saez-Atienzar, S. *et al.* The LRRK2 inhibitor GSK2578215A induces protective autophagy in SH-SY5Y cells: involvement of Drp-1-mediated mitochondrial fission and mitochondrial-derived ROS signaling. *Cell Death Dis.* **5,** e1368 (2014).

97. Manzoni, C. *et al.* mTOR independent regulation of macroautophagy by Leucine Rich Repeat Kinase 2 via Beclin-1. *Sci. Rep.* **6,** 35106 (2016).

98. Sánchez-Danés, A. *et al.* Disease-specific phenotypes in dopamine neurons from human iPS-based models of genetic and sporadic Parkinson's disease. *EMBO Mol. Med.* **4,** 380–395 (2012).

99. Manzoni, C. LRRK2 and autophagy: a common pathway for disease. *Biochem. Soc. Trans.* **40,** 1147–51 (2012).

100. Jellinger, K. A. Recent advances in our understanding of neurodegeneration. *J. Neural Transm.* **116,** 1111–1162 (2009).

101. Falcone, C. & Mazzoni, C. External and internal triggers of cell death in yeast. *Cell. Mol. Life Sci.* **73,** 2237–2250 (2016).

102. Eisenberg, T., Büttner, S., Kroemer, G. & Madeo, F. The mitochondrial pathway in yeast apoptosis. *Apoptosis* **12,** 1011–1023 (2007).

103. Haynes, C. M., Titus, E. A. & Cooper, A. A. Degradation of Misfolded Proteins

Prevents ER-Derived Oxidative Stress and Cell Death. *Mol. Cell* **15,** 767–776 (2004).

104. Braun, R. J., Büttner, S., Ring, J., Kroemer, G. & Madeo, F. Nervous yeast: modeling neurotoxic cell death. *Trends Biochem. Sci.* **35,** 135–144 (2010).

105. Franssens, V. *et al.* Yeast unfolds the road map toward α-synuclein-induced cell death. *Cell Death Differ.* **17,** 746–753 (2010).

106. Xiong, Y. *et al.* GTPase activity plays a key role in the pathobiology of LRRK2. *PLoS Genet.* **6,** (2010).

107. Xiong, Y., Yuan, C., Chen, R., Dawson, T. M. & Dawson, V. L. ArfGAP1 Is a GTPase Activating Protein for LRRK2: Reciprocal Regulation of ArfGAP1 by LRRK2. *J. Neurosci.* **32,** 3877–3886 (2012).

108. Stafa, K. *et al.* GTPase Activity and Neuronal Toxicity of Parkinson's Disease–Associated LRRK2 Is Regulated by ArfGAP1. *PLoS Genet.* **8,** e1002526 (2012).

109. Pereira, C., Miguel Martins, L. & Saraiva, L. LRRK2, but not pathogenic mutants, protects against H2O2 stress depending on mitochondrial function and endocytosis in a yeast model. *Biochim. Biophys. Acta - Gen. Subj.* **1840,** 2025–2031 (2014).

110. Gómez-Suaga, P., Churchill, G. C., Patel, S. & Hilfiker, S. A link between LRRK2, autophagy and NAADP-mediated endolysosomal calcium signalling. *Biochem. Soc. Trans.* **40,** 1140–6 (2012).

111. Yang, Z. & Klionsky, D. J. An overview of the molecular mechanism of autophagy. *Curr. Top. Microbiol. Immunol.* **335,** 1–32 (2009).

112. Reggiori, F. & Klionsky, D. J. Autophagic processes in yeast: Mechanism, machinery and regulation. *Genetics* **194,** 341–361 (2013).

113. Galluzzi, L. *et al.* Molecular definitions of autophagy and related processes. *EMBO J.* **36,** 1811–1836 (2017).

114. Dikic, I. Proteasomal and Autophagic Degradation Systems. *Annu. Rev. Biochem.* **86,** 193–224 (2017).

115. Suzuki, K. *et al.* The pre-autophagosomal structure organized by concerted functions of APG genes is essential for autophagosome formation. *EMBO J.* **20,** 5971–5981 (2001).

116. Burman, C. & Ktistakis, N. T. Regulation of autophagy by phosphatidylinositol 3-phosphate. *FEBS Lett.* **584,** 1302–1312 (2010).

117. Wen, X. & Klionsky, D. J. An overview of macroautophagy in yeast. *J. Mol. Biol.* **428,** 1681–99 (2016).

118. Geng, J. & Klionsky, D. J. The Atg8 and Atg12 ubiquitin-like conjugation systems in macroautophagy. 'Protein Modifications: Beyond the Usual Suspects' Review Series. *EMBO Rep.* **9,** 859–864 (2008).

119. Shintani, T. *et al.* Apg10p, a novel protein-conjugating enzyme essential for autophagy in yeast. *EMBO J.* **18,** 5234–5241 (1999).

120. Romanov, J. *et al.* Mechanism and functions of membrane binding by the Atg5-Atg12/Atg16 complex during autophagosome formation. *EMBO J.* **31,** 4304–4317 (2012).

121. Ichimura, Y. *et al.* A ubiquitin-like system mediates protein lipidation. *Nature* **408,** 488–492 (2000).

122. Kaufmann, A., Beier, V., Franquelim, H. G. & Wollert, T. Molecular Mechanism of Autophagic Membrane-Scaffold Assembly and Disassembly. *Cell* **156,** 469–481 (2014).

123. Yamamoto, H. *et al.* Atg9 vesicles are an important membrane source during early steps of autophagosome formation. *J. Cell Biol.* **198,** 219–233 (2012).

124. Baba, M., Osumi, M., Scott, S. V, Klionsky, D. J. & Ohsumi, Y. Two distinct pathways for targeting proteins from the cytoplasm to the vacuole/lysosome. *J. Cell Biol.* **139,** 1687–95 (1997).

125. Balderhaar, H. J. kleine *et al.* The Rab GTPase Ypt7 is linked to retromer-mediated receptor recycling and fusion at the yeast late endosome. *J. Cell Sci.* **123,** 4085–4094 (2010).

126. Darsow, T., Rieder, S. E. & Emr, S. D. A multispecificity syntaxin homologue,

Vam3p, essential for autophagic and biosynthetic protein transport to the vacuole. *J. Cell Biol.* **138,** 517–29 (1997).

127. Takeshige, K., Baba, M., Tsuboi, S., Noda, T. & Ohsumi, Y. Autophagy in yeast demonstrated with proteinase-deficient mutants and conditions for its induction. *J. Cell Biol.* **119,** 301–11 (1992).

128. Epple, U. D., Suriapranata, I., Eskelinen, E.-L. & Thumm, M. Aut5/Cvt17p, a Putative Lipase Essential for Disintegration of Autophagic Bodies inside the Vacuole. *J. Bacteriol.* **183,** 5942–5955 (2001).

129. Loewith, R. & Hall, M. N. Target of rapamycin (TOR) in nutrient signaling and growth control. *Genetics* **189,** 1177–201 (2011).

130. Cebollero, E. & Reggiori, F. Regulation of autophagy in yeast Saccharomyces cerevisiae. *Biochim. Biophys. Acta - Mol. Cell Res.* **1793,** 1413–1421 (2009).

131. De Virgilio, C. & Loewith, R. Cell growth control: little eukaryotes make big contributions. *Oncogene* **25,** 6392–6415 (2006).

132. Schmidt, A., Kunz, J. & Hall, M. N. TOR2 is required for organization of the actin cytoskeleton in yeast. *Proc. Natl. Acad. Sci. U. S. A.* **93,** 13780–5 (1996).

133. Kamada, Y. *et al.* Tor Directly Controls the Atg1 Kinase Complex To Regulate Autophagy. *Mol. Cell. Biol.* **30,** 1049–1058 (2010).

134. Kamada, Y. *et al.* Tor-mediated induction of autophagy via an Apg1 protein kinase complex. *J. Cell Biol.* **150,** 1507–13 (2000).

135. Li, S. C. & Kane, P. M. The yeast lysosome-like vacuole: endpoint and crossroads. *Biochim. Biophys. Acta* **1793,** 650–63 (2009).

136. Hecht, K. A., O'Donnell, A. F. & Brodsky, J. L. The proteolytic landscape of the yeast vacuole. *Cell. Logist.* **4,** e28023 (2014).

137. Jefferies, K. C., Cipriano, D. J. & Forgac, M. Function, structure and regulation of the vacuolar (H+)-ATPases. *Arch. Biochem. Biophys.* **476,** 33–42 (2008).

138. Matsumoto, R., Suzuki, K. & Ohya, Y. Organelle acidification is important for localisation of vacuolar proteins in Saccharomyces cerevisiae. *Protoplasma* **250,**

1283–1293 (2013).

139. Van Den Hazel, H. B., Kielland-Brandt, M. C. & Winther, J. R. Review: biosynthesis and function of yeast vacuolar proteases. *Yeast* **12,** 1–16 (1996).

140. Westphal, V., Marcusson, E. G., Winther, J. R., Emr, S. D. & van den Hazel, H. B. Multiple pathways for vacuolar sorting of yeast proteinase A. *J. Biol. Chem.* **271,** 11865–70 (1996).

141. van den Hazel, H. B., Kielland-Brandt, M. C. & Winther, J. R. Autoactivation of proteinase A initiates activation of yeast vacuolar zymogens. *Eur. J. Biochem.* **207,** 277–83 (1992).

142. Carmona-Gutierrez, D. & Büttner, S. The many ways to age for a single yeast cell. *Yeast* **31,** 289–98 (2014).

143. Aufschnaiter, A. *et al.* The Coordinated Action of Calcineurin and Cathepsin D Protects Against α-Synuclein Toxicity. *Front. Mol. Neurosci.* **10,** 207 (2017).

144. Carmona-Gutiérrez, D. *et al.* The propeptide of yeast cathepsin D inhibits programmed necrosis. *Cell Death Dis.* **2,** e161 (2011).

145. Büttner, S. *et al.* Functional mitochondria are required for ??-synuclein toxicity in aging yeast. *J. Biol. Chem.* **283,** 7554–7560 (2008).

146. Schindelin, J. *et al.* Fiji: an open-source platform for biological-image analysis. *Nat. Methods* **9,** 676–682 (2012).

147. Yee, B., Tsuyumu, S. & Adams, B. G. Biological effects of dimethyl sulfoxide on yeast. *Biochem. Biophys. Res. Commun.* **49,** 1336–1342 (1972).

148. Sadowska-Bartosz, I., Pączka, A., Mołoń, M. & Bartosz, G. Dimethyl sulfoxide induces oxidative stress in the yeast *Saccharomyces cerevisiae*. *FEMS Yeast Res.* **13,** 820–830 (2013).

149. Klionsky, D. J. *et al.* Guidelines for the use and interpretation of assays for monitoring autophagy (3rd edition). *doi.org* 1–222 (2016). doi:10.1080/15548627.2015.1100356

150. Weidberg, H., Shvets, E. & Elazar, Z. Biogenesis and Cargo Selectivity of

Autophagosomes. *Annu. Rev. Biochem.* **80,** 125–156 (2011).

151. Madeo, F., Eisenberg, T., Büttner, S., Ruckenstuhl, C. & Kroemer, G. Spermidine: a novel autophagy inducer and longevity elixir. *Autophagy* **6,** 160–2 (2010).

152. Decuypere, J. P., Bultynck, G. & Parys, J. B. A dual role for Ca2+ in autophagy regulation. *Cell Calcium* **50,** 242–250 (2011).

153. Büttner, S. *et al.* The Ca2+/Mn2+ ion-pump PMR1 links elevation of cytosolic Ca(2+) levels to α-synuclein toxicity in Parkinson's disease models. *Cell Death Differ.* **20,** 465–77 (2013).

154. Sevlever, D., Jiang, P. & Yen, S.-H. C. Cathepsin D is the main lysosomal enzyme involved in the degradation of alpha-synuclein and generation of its carboxy-terminally truncated species. *Biochemistry* **47,** 9678–87 (2008).

155. Qiao, L. *et al.* Lysosomal enzyme cathepsin D protects against alpha-synuclein aggregation and toxicity. *Mol. Brain* **1,** 17 (2008).

156. Matrone, C. *et al.* Mannose 6-Phosphate Receptor Is Reduced in -Synuclein Overexpressing Models of Parkinsons Disease. *PLoS One* **11,** e0160501 (2016).

157. Winslow, A. R. *et al.* α-Synuclein impairs macroautophagy: implications for Parkinson's disease. *J. Cell Biol.* **190,** 1023–37 (2010).

158. Greggio, E., Bisaglia, M., Civiero, L. & Bubacco, L. Leucine-rich repeat kinase 2 and alpha-synuclein: intersecting pathways in the pathogenesis of Parkinson's disease? *Mol Neurodegener* **6,** 6 (2011).

159. Cooper, A. A. *et al.* Alpha-synuclein blocks ER-Golgi traffic and Rab1 rescues neuron loss in Parkinson's models. *Science* **313,** 324–8 (2006).

160. Büttner, S. *et al.* Functional Mitochondria Are Required for α-Synuclein Toxicity in Aging Yeast. *J. Biol. Chem.* **283,** 7554–7560 (2008).

161. Büttner, S. *et al.* Endonuclease G mediates α-synuclein cytotoxicity during Parkinson's disease. *EMBO J.* **32,** 3041–54 (2013).

162. Zabrocki, P. *et al.* Characterization of α-synuclein aggregation and synergistic

toxicity with protein tau in yeast. *FEBS J.* **272,** 1386–1400 (2005).

163. Carmona-Gutiérrez, D. *et al.* The propeptide of yeast cathepsin D inhibits programmed necrosis. *Cell Death Dis.* **2,** e161 (2011).

164. Moors, T. *et al.* Lysosomal Dysfunction and α-Synuclein Aggregation in Parkinson's Disease: Diagnostic Links. *Mov. Disord.* **31,** 791–801 (2016).

165. Høyer-Hansen, M. *et al.* Control of Macroautophagy by Calcium, Calmodulin-Dependent Kinase Kinase-β, and Bcl-2. *Mol. Cell* **25,** 193–205 (2007).

166. Gastaldello, A., Callaghan, H., Gami, P. & Campanella, M. Ca^{2+} -dependent autophagy is enhanced by the pharmacological agent PK11195. *Autophagy* **6,** 607–613 (2010).

167. Grotemeier, A. *et al.* AMPK-independent induction of autophagy by cytosolic Ca2+ increase. *Cell. Signal.* **22,** 914–925 (2010).

168. Harr, M. W., McColl, K. S., Zhong, F., Molitoris, J. K. & Distelhorst, C. W. Glucocorticoids downregulate Fyn and inhibit IP3-mediated calcium signaling to promote autophagy in T lymphocytes. *Autophagy* **6,** 912–921 (2010).

169. Eisenberg, T. *et al.* Induction of autophagy by spermidine promotes longevity. *Nat. Cell Biol.* **11,** 1305–1314 (2009).

170. Li, J., Kim, S. G. & Blenis, J. Rapamycin: one drug, many effects. *Cell Metab.* **19,** 373–9 (2014).

171. Bové, J., Martínez-Vicente, M. & Vila, M. Fighting neurodegeneration with rapamycin: mechanistic insights. *Nat. Rev. Neurosci.* **12,** 437–452 (2011).

172. Malagelada, C., Jin, Z. H., Jackson-Lewis, V., Przedborski, S. & Greene, L. A. Rapamycin protects against neuron death in in vitro and in vivo models of Parkinson's disease. *J. Neurosci.* **30,** 1166–75 (2010).

173. Dehay, B. *et al.* Pathogenic Lysosomal Depletion in Parkinson's Disease. *J. Neurosci.* **30,** 12535–12544 (2010).

174. Decressac, M. *et al.* TFEB-mediated autophagy rescues midbrain dopamine neurons from α-synuclein toxicity. *Proc. Natl. Acad. Sci. U. S. A.* **110,** E1817-26

(2013).

175. Hebron, M. L., Lonskaya, I. & Moussa, C. E.-H. Nilotinib reverses loss of dopamine neurons and improves motor behavior via autophagic degradation of α-synuclein in Parkinson's disease models. *Hum. Mol. Genet.* **22,** 3315–28 (2013).

176. Chen, L.-L. *et al.* Corynoxine, a Natural Autophagy Enhancer, Promotes the Clearance of Alpha-Synuclein via Akt/mTOR Pathway. *J. Neuroimmune Pharmacol.* **9,** 380–387 (2014).

177. Anglade, P. *et al.* Apoptosis and autophagy in nigral neurons of patients with Parkinson's disease. *Histol. Histopathol.* **12,** 25–31 (1997).